

# The $\kappa$ -cookbook: a novel generalizing approach to unify $\kappa$ -like distributions for plasma particle modeling

K. Scherer,<sup>1,2\*</sup> and E. Husidic<sup>1,3</sup>, M. Lazar,<sup>1,3</sup>, H. Fichtner,<sup>1,2</sup>

<sup>1</sup>*Institut für Theoretische Physik, Lehrstuhl IV: Plasma-Astroteilchenphysik, Ruhr-Universität Bochum, D-44780 Bochum, Germany*

<sup>2</sup>*Research Department, Plasmas with Complex Interactions, Ruhr-Universität Bochum, 44780 Bochum, Germany*

<sup>3</sup>*Centre for Mathematical Plasma Astrophysics, 3001 Leuven Belgium*

## ABSTRACT

In the literature different so-called  $\kappa$ -distribution functions are discussed to fit and model the velocity (or energy) distributions of solar wind species, pickup ions or magnetospheric particles. Here we introduce a generalized (isotropic)  $\kappa$ -distribution as a "cookbook", which admits as special cases, or "recipes", all the other known versions of  $\kappa$ -models. A detailed analysis of the generalized distribution function is performed, providing general analytical expressions for the velocity moments, Debye length, and entropy, and pointing out a series of general requirements that plasma distribution functions should satisfy. From a contrasting analysis of the recipes found in the literature, we show that all of them lead to almost the same macroscopic parameters with a small standard deviation between them. However, one of these recipes called the regularized  $\kappa$ -distribution provides a functional alternative for macroscopic parameterization without any constraint for the power-law exponent  $\kappa$ .

**Key words:** plasmas, Sun: heliosphere, solar wind, methods: data analysis

## 1 INTRODUCTION

Different so-called Kappa- or  $\kappa$ -distributions are widely applied in space physics to model the suprathermal tails of particle energy or velocity distributions in collision-poor and dilute astrophysical plasma environments. While the core of such distributions can be well fitted by a Maxwellian, the enhanced wings of the distribution are best approximated by power-laws (Pierrard & Lazar 2010). The original  $\kappa$ -distribution has been defined over 50 years ago in a rather ad-hoc manner by Olbert (1968) and Vasyliunas (1968) to reproduce the velocity distributions of magnetospheric electrons. Since then various attempts have been made to derive the  $\kappa$ -distribution theoretically in a more rigorous way in prescribed plasma setups, e.g., Hasegawa et al. (1985), who derived a Kappa-like energy distribution for a plasma in a superthermal radiation field, Ma & Summers (1998), who found a  $\kappa$ -distribution to be the solution of the Fokker-Planck equation with the inclusion of stationary whistler turbulence, and Yoon (2014), who self-consistently solved

the problem of an isotropic electron distribution that is in equilibrium with the electrostatic Langmuir turbulence and found a  $\kappa$ -distribution with specifically  $\kappa = 9/4$  (see below for an explanation of the  $\kappa$ -parameter). Further effort to put the  $\kappa$ -distributions on a more solid theoretical ground resulted in a generalization of the standard Boltzmann-Gibbs entropy by Tsallis (1988) and Treumann & Jaroschek (2008) in order to account for non-equilibrium distributions and a nonadditive entropy (see also Fichtner et al. 2018).

Besides its original employment by Olbert (1968) and Vasyliunas (1968) to describe electrons in Earth's magnetosphere, the family of  $\kappa$ -distributions finds practical application also in many other areas of space physics, e.g., in the study of the interplanetary medium and planetary magnetospheres (Maksimovic et al. 1997, 2005; Pierrard & Lazar 2010), the outer heliosphere (Zank et al. 2010; Fahr et al. 2016, 2017; Heerikhuisen et al. 2019), especially for charge exchange processes (Heerikhuisen et al. 2015) and to fit IBEX observations of neutral atoms (Desai et al. 2012), the interstellar medium (Davelaar et al. 2018) and the intergalactic medium (de Avillez et al. 2018). Recently the  $\kappa$ -

\* kls@was.tp4.rub.de

distributions found their way even into experimental physics (Webb et al. 2012; Elkamash & Kourakis 2016).

Following the terminology in Scherer et al. (2017a, 2019a) we will call the original version by Vasylunas (1968) the standard  $\kappa$ -distribution (SKD), defined as

$$f_{SKD}(\vec{r}, \vec{v}, t) = \frac{n(\vec{r}, t)}{\sqrt{\pi^3} \kappa \Theta^3} \frac{\Gamma(\kappa)}{\Gamma(\kappa - \frac{1}{2})} \left[ 1 + \frac{v^2}{\kappa \Theta^2} \right]^{-(\kappa+1)}, \quad (1)$$

where  $\Gamma(\mu)$  is the (complete) Gamma function of argument  $\mu$ ,  $\Theta$  is defined as the most probable speed, which normalizes the particle velocity  $\vec{v}$  and its magnitude  $v$ , respectively, and  $n(\vec{r}, t)$  is the number density, which in general can depend on location  $\vec{r}$  and time  $t$ . The  $\kappa$ -parameter is a free parameter and serves as a measure of the departure of the SKD from its Maxwellian core (Vasylunas 1968) and thus describes the high-energy power-law tails of the distribution. Equation (1) and all the following specified distributions are normalized to number density, and for  $\kappa \rightarrow \infty$  the SKD approaches its Maxwellian core. Beside the SKD many other  $\kappa$ -like versions have been proposed in the literature (e.g., Yoon 2012; Livadiotis & McComas 2013; Lazar et al. 2015; Treumann & Baumjohann 2014; Lazar et al. 2017; Scherer et al. 2017b), of which most suffer under one or more deficiencies listed in the next paragraph. Some authors use  $-\kappa$  (Yoon 2014; Pierrard et al. 2016) as the exponent of the square bracket in Eq. (1) or  $\kappa - \frac{3}{2}$  in the denominator (Livadiotis & McComas 2013) in the square bracket in Eq. (1), with various arguments relying in general on physical or theoretical implications of the velocity moments of Eq. 1.

Despite its frequent successful employment, the SKD introduces certain unphysical characteristics. The major deficiency of the SKD is the existence of diverging velocity moments, which prevents establishing a fully consistent macroscopic non-equilibrium plasma model. For the  $l$ th velocity moment to exist,  $\kappa$  must fulfill the condition  $\kappa > (l+1)/2$  (Scherer et al. 2017a). The definition of kinetic temperature from the second-order moment of the SKD restricts the spectral power to  $\kappa > 3/2$ . Furthermore, Scherer et al. (2019b) showed that for values of  $\kappa < 2$  superluminal particles with  $v > c$ , (with  $c$  the speed of light), contribute significantly to macroscopic quantities like the pressure or entropy. The concept of a non-additive entropy mentioned above is also still controversial (see, e.g., the exchange between Nauenberg (2003); Tsallis (2004); Nauenberg (2004) and the discussion in Fichtner et al. (2018)). For the SKD there is also some discrepancy regarding the Debye length: for example, while Mace et al. (1998) and Livadiotis & McComas (2004) derive a vanishing Debye length for  $\kappa \rightarrow 3/2$ , Treumann et al. (2004) find it to diverge in this limit, and Fahr & Heyl (2016) determine it to be ten times that of the associated Maxwellian plasma.

An important progress has been made by introducing the regularized  $\kappa$ -distribution (RKD), which admits a divergence-free macroscopic moment parameterization without any restriction for the power-index  $\kappa$  (Scherer et al. 2017b, 2019b). The RKD is defined as

$$f_{RKD}(\vec{r}, \vec{v}, t) = \frac{n(\vec{r}, t)}{\sqrt{\pi^3} \Theta^3} \frac{1}{\sqrt{\kappa^3} U(\frac{3}{2}, \frac{3}{2} - \kappa, \alpha^2 \kappa)} \left( 1 + \frac{v^2}{\kappa \Theta^2} \right)^{-(\kappa+1)} e^{-\alpha^2 \frac{v^2}{\Theta^2}}, \quad (2)$$

where  $U(a, c, x)$  is the Kummer- $U$  or Tricomi function and  $\alpha$  is the cutoff-parameter, which reproduces the SKD for  $\alpha = 0$ . The characteristics and physical implications of the RKD are still explored, e.g., regarding the pressure and heat flux (Lazar et al. 2019) or the dispersion properties (Husidic et al. 2020) in RKD-plasmas.

In literature we do find not only the standard/regularized  $\kappa$ -distributions, but also some extensions. To date there is no consensus about a universally accepted version or interpretation of the  $\kappa$ -distributions (see, e.g., Lazar et al. (2015) and Livadiotis (2015) and references therein). In our present work we unify all these attempts and propose a straightforward generalization of the  $\kappa$ -distributions, which we will call the  $\kappa$ -cookbook. From it all the already-known  $\kappa$ -distributions can be derived, which we will call recipes (see in Section 2 for a detailed definition). Moreover, we can provide general analytical expressions for the velocity moments, the Debye length and the entropy, and compare the results for the different recipes to analyze their mathematical and physical significance. A further comparison can be achieved by fitting the recipes to real data, for which we use an electron data set by the ESA space probe Ulysses from an event on February 15, 2002, when Ulysses was in its second orbit around the Sun (Marsden & Smith 2003). We demonstrate that the discussed recipes lead to almost the same values for the macroscopic moments and give easy to use formulas for the velocity moments of the generalized kappa distributions, which can be used in future without performing the explicit integration of the velocity moments.

The paper is organized as follows. In Section 2 we introduce a generalized  $\kappa$ -distribution, which enables a rather general derivation of the moments, the Debye length, and the entropy. Having these general formulations at hand, we discuss more properties in Section 3, while some specific recipes are analyzed in detail in Section 4. In Section 5 we consider some examples commonly used in the literature, and discuss the impact of choosing them as recipes of our  $\kappa$ -cookbook. An examination of higher-order moments follows in Section 6, while in Section 7 we take a closer look at the Debye length for each relevant recipe. Finally, we apply the discussed recipes to observations in Section 8, and end with a summary and conclusions in Section 9.

## 2 THE $\kappa$ -COOKBOOK

Before we introduce the generalized  $\kappa$ -distribution (GKD), we briefly mention that all distribution functions must obey the same physical laws, that are those derived from the Liouville theorem (e.g., Balescu 1988). Hence the H-theorem holds and the entropy is finite and extensive. Furthermore, we take it for granted that the contribution of superluminal particles is negligible (see Scherer et al. 2019a). Moreover, it is required that the Debye length  $\Lambda$  is finite and positive. Thus, in short, a well-posed distribution function in plasma physics must obey the following rules, restricted to the case where the phase space volume is conserved:

1. The distribution function should fulfill the Liouville theorem. Here we restrict ourselves to the case that it should be an (approximate) solution of the Vlasov equation (e.g. Balescu 1988).

2. All moments must exist (e.g. Schwabl 2013).
3. The entropy is given via the H-theorem (e.g. Balescu 1988).
4. The plasma parameter  $N_p = \frac{4\pi}{3}n_0\Lambda^3$  must be high (e.g. Goedbloed et al. 2010), where  $N_p$  gives the number of particles in a Debye sphere and  $n_0$  is the number density.
5. The contribution of superluminal particles shall be negligible (Scherer et al. 2019a).

There can be other restrictions, but for our purposed dealing with classical plasma distribution functions, the above conditions are necessary (see also below).

In the following we study a generalized form of the isotropic regularized  $\kappa$ -distribution (RKD), which we call the "cookbook":

$$f_{GKD}(\eta, \zeta, \xi, v) \equiv n_0 N_G \left(1 + \frac{v^2}{\eta(\kappa)\Theta^2}\right)^{-\zeta(\kappa)} e^{-\xi(\kappa)\frac{v^2}{\Theta^2}} \quad (3)$$

with  $\eta(\kappa), \zeta(\kappa), \xi(\kappa) \in \mathbb{R}_+$ ,

and specific values of  $\eta \equiv \eta(\kappa)$ ,  $\zeta \equiv \zeta(\kappa)$  and  $\xi \equiv \xi(\kappa)$  are called the "recipes" given by the tuple  $(\eta, \zeta, \xi)$ .  $N_G$  is the normalization constant (see below Eq. 7). We will discuss a selection of recipes below.

To save writing we introduce similar to our earlier definition (Scherer et al. 2019b)

$${}^{[m]}\mathcal{W}^{[n]}(\eta, \zeta, \xi) = \frac{U\left(\frac{3+m}{2}, \frac{5+m}{2} - \zeta, \xi\eta\right)}{U\left(\frac{3+n}{2}, \frac{5+n}{2} - \zeta, \xi\eta\right)}. \quad (4)$$

where  $n, m$  are arbitrary velocity moments. Because we only will need the ratios for  $n=0$ , we may further write

$${}^{[m]}\mathcal{W}(\eta, \zeta, \xi) = \frac{U\left(\frac{3+m}{2}, \frac{5+m}{2} - \zeta, \xi\eta\right)}{U\left(\frac{3}{2}, \frac{5}{2} - \zeta, \xi\eta\right)}. \quad (5)$$

First we give further ingredients of the  $\kappa$ -cookbook, namely the velocity moments, i.e., the  $n$ th order moment  $M_n$ , the normalization constant  $N_G$ , the most probable speed  $v_p$ , and the pressure  $P$  (see Appendix B).

$$M_n = 2\pi n_0 N_G \eta^{\frac{3+n}{2}} \Theta^{3+n} \Gamma\left(\frac{n+3}{2}\right) U\left(\frac{n+3}{2}, \frac{n+5}{2} - \zeta, \xi\eta\right) = \frac{2n_0}{\sqrt{\pi}} \eta^{\frac{n}{2}} \Theta^n \Gamma\left(\frac{n+3}{2}\right) {}^{[n]}\mathcal{W}(\eta, \zeta, \xi) \quad (6)$$

$$N_G^{-1} = \frac{M_0}{n_0} = \eta \Theta^3 \sqrt{\pi^3} U\left(\frac{3}{2}, \frac{5}{2} - \zeta, \xi\eta\right) \quad (7)$$

$$v_p = M_1 = \frac{2n_0\Theta}{\sqrt{\pi}} \eta^{\frac{1}{2}} {}^{[1]}\mathcal{W}(\eta, \zeta, \xi) \quad (8)$$

$$P = M_2 = \frac{2n_0\Theta^2}{3} \eta {}^{[2]}\mathcal{W}(\eta, \zeta, \xi). \quad (9)$$

With the approach by Krall & Trivelpiece (1973) (see Appendix C1) we estimate the Debye length  $\Lambda$  to

$$\Lambda^2 = \Lambda_0^2 \tilde{\Lambda}^2 = \frac{1}{2} \Lambda_0^2 \left[ \frac{\zeta}{\eta} \frac{U\left(\frac{3}{2}, \frac{3}{2} - \zeta, \eta\xi\right)}{U\left(\frac{3}{2}, \frac{5}{2} - \zeta, \eta\xi\right)} + \xi \right]^{-1} \quad (10)$$

with

$$\Lambda_0^2 = \frac{\epsilon_0 m_s \Theta_s^2}{n_s q_s^2}, \quad (11)$$

$$\tilde{\Lambda}^2 = \frac{1}{2} \left[ \frac{\zeta}{\eta} \frac{U\left(\frac{3}{2}, \frac{3}{2} - \zeta, \eta\xi\right)}{U\left(\frac{3}{2}, \frac{5}{2} - \zeta, \eta\xi\right)} + \xi \right]^{-1},$$

where the factor 2 comes from the fact that usually a Maxwellian is defined replacing  $\Theta^2$  with the thermal speed and a factor 2:  $\Theta^2 = 2v_p^2$ . In Eq. (11)  $m_s$  denotes the mass and  $q_s$  the charge of particle species  $s$ , and  $\epsilon_0$  is the vacuum permittivity.

We will use the entropy  $S$  (Appendix B1) only in its normalized version  $\tilde{S} = S/(4\pi N k_B)$  (with the Boltzmann constant  $k_B$  and the total number of particles  $N$ ). By omitting the Gibbs correction (see for example Fichtner et al. 2018), we find for the entropy

$$\tilde{S} = -\ln n_0 + 3 \ln \Theta + \ln \left[ \eta^{\frac{3}{2}} \sqrt{\pi^3} U\left(\frac{3}{2}, \frac{5}{2} - \zeta, \xi\eta\right) \right] + \frac{\zeta}{2\pi} \sum_{l=0}^{\infty} \frac{1}{l+1} \frac{U\left(\frac{3}{2}, \frac{3}{2} - \zeta - l, \eta\xi\right)}{U\left(\frac{3}{2}, \frac{5}{2} - \zeta, \eta\xi\right)} + \frac{2\xi\eta}{3} {}^{[2]}\mathcal{W}(\eta, \zeta, \xi). \quad (12)$$

From Eq. (12) it is not directly evident that this non-equilibrium entropy is lower than the classical equilibrium entropy discussed in thermodynamics (e.g. Schwabl 2013), but for the corresponding Maxwellian we have to choose the correct temperature, e.g., the one given by the cookbook, and then it can be shown that it is lower than the equilibrium entropy (see Scherer et al. 2019b, for the RKD case).

We can obtain the Maxwellian distribution function  $f^M$  and the corresponding moments  $M_n^M$  with the recipe  $(\eta > 0, \zeta = 0, \xi = 1)$ , for a more detailed discussion see Section 4.1. It turns out that the general moments can be written as a product of the Maxwellian moments and a "correction" factor  $\tilde{M}$ :

$$M_n = M_n^M \tilde{M} \quad \text{with} \quad \begin{cases} \tilde{M} \equiv \eta^{\frac{n}{2}} {}^{[n]}\mathcal{W} \\ M_n^M = \frac{2}{\sqrt{\pi}} \Theta^n \Gamma\left(\frac{n+3}{2}\right). \end{cases} \quad (13)$$

Analogously, we define  $\tilde{v}_p$  and  $\tilde{P}$  as the most probable speed and pressure, respectively. In an analogous way we can define the distribution function

$$f = N_M \tilde{f} \quad \text{with} \quad \begin{cases} \tilde{f} \equiv \frac{1}{\eta^{\frac{3}{2}} \sqrt{\pi^3}} \frac{\left(1 + \frac{v^2}{\eta\Theta^2}\right)^{-\zeta} e^{-\xi\frac{v^2}{\Theta^2}}}{U\left(\frac{3}{2}, \frac{5}{2} - \zeta, \eta\xi\right)} \\ N_M = \frac{n_0}{\Theta^3} \end{cases} \quad (14)$$

with a "Maxwellian" normalization  $N_M$ . In the following we do not take into account the Maxwellian part, but rather study the normalized distribution functions and their moments.

### 3 SOME GENERAL PROPERTIES

It is obvious that for  $\{\eta(\kappa), \zeta(\kappa), \xi(\kappa)\} \in \mathbb{R}_+$  the first three conditions are fulfilled, the fourth condition needs to be checked, because it depends also on the number density, and the fifth condition is fulfilled when  $\xi > \frac{\Theta^2}{c^2}$ , where  $c$  is the speed of light. More interesting are the cases when one or more of the parameters  $(\eta, \zeta, \xi)$  are zero. This can be the case if they are strictly zero, or if they vanish for a given  $(\kappa)$ -value. First, we discuss the case when they are

strictly zero, because the other case can be deduced from the former. In the last subsection, we study the recipes ( $\eta \rightarrow 0, \zeta \neq 0, \xi \rightarrow \infty$ ), which can appear when replacing  $\xi$  by  $\eta^{-1}\xi$  as used by DeStefano (2019).

In the following we discuss some special recipes, i.e., ( $\eta > 0, \zeta = 0, \xi \neq 0$ ) the Maxwellian, ( $\eta \neq 0, \zeta \neq 0, \xi = 0$ ) the SKD, and ( $\eta = 0, \zeta \neq 0, \xi \neq 0$ ). Furthermore, instead of using the shorthand notations SKD and RKD, we will mainly use the corresponding recipes. We study first some general properties of the GKD with finite and positive recipes, meaning that each parameter of tuple  $(\eta, \zeta, \xi)$  is finite and positive (Section 3.1 below), and then the recipes, where one or more of the parameters vanishes (Section 4).

### 3.1 The form of the distribution function $\tilde{f}$

For this section we make the assumption that  $\{\eta(\kappa), \zeta(\kappa), \xi(\kappa)\} \in \mathcal{R}_+$ . Inserting the normalization constant  $N_G$  in Eq. (3) and neglecting the Maxwellian part, see Eq. (14), leads to

$$\tilde{f} = \underbrace{\frac{1}{\eta^{\frac{3}{2}} U\left(\frac{3}{2}, \frac{5}{2} - \zeta, \eta \xi\right)}}_{\text{the normalization}} \underbrace{\left(1 + \frac{v^2}{\eta(\kappa)\Theta^2}\right)^{-\zeta(\kappa)}}_{\text{the form}} \underbrace{e^{-\xi(\kappa)\frac{v^2}{\Theta^2}}}_{\text{the cutoff}}, \quad (15)$$

which has been decomposed into the above three parts. The form part will be decomposed further in a part describing the tail flatness, depending on  $\zeta$ , and a part describing the form of the peak. This is illustrated in Fig. 3.1, where we show in the left upper panel the standard RKD, and in the upper middle and right panel we vary  $\zeta$  for  $\eta = \kappa$ , while in the lower left and middle panel we vary  $\eta$  for  $\zeta = \kappa + 1$ , and finally in the lower right panel we change both  $\zeta$  and  $\eta$ . The corresponding recipes are given in Table 3. We have only plotted the low values of  $v/\Theta$  so that the cutoff parameter  $\xi = 0.1^2$  does not play a role, and thus the figures for lower  $\xi < 0.1^2$  will look very similar and need not be included in the above discussion.

Comparing the RKD with the recipe  $(\kappa, \kappa, 0.1^2)$  shows that the tails of the latter are much flatter than those of the RKD and vice versa for the recipe  $(\kappa, \kappa + 2, 0.1^2)$ , which has steeper tails than the RKD. That is the reason why we call the parameter  $\zeta$  the flatness parameter.

Keeping  $\zeta = \kappa + 1$  and changing the  $\eta$ -parameter shows that it influences the shape of the peak: The peaks for the recipe  $(\kappa + 5, \kappa + 1, 0.1^2)$  and for  $(2\kappa, \kappa + 1, 0.1^2)$  are flatter than that of the RKD. Finally, in the last panel we show how both parameters influence the form of the recipe  $(\kappa + 5, \kappa, 0.1^2)$ .

The discussed recipes (Table 3) or similar ones can be used to fit a distribution function to data, but do not say anything about the necessary physical conditions. This we will discuss in quite general form in the next section.

## 4 ZERO-RECIPES

### 4.1 The recipes with $\zeta = 0$

With the choice of  $(\eta, \zeta, \xi) = (1, 0, 1)$  we get the standard Maxwellian distributions (up to a factor 2 when comparing

$\Theta$  with the thermal speed) and the corresponding moments from Eq. (6):

$$M_n^M = \frac{2n_0}{\sqrt{\pi}} \Theta^n \Gamma\left(\frac{n+3}{2}\right) \underbrace{\frac{U\left(\frac{n+3}{2}, \frac{n+5}{2}, 1\right)}{U\left(\frac{3}{2}, \frac{5}{2}, 1\right)}}_{=1} \quad (16)$$

(see Appendix, Eq. (A5)). Comparing this with the general moments we have always a part, which is analogous to the Maxwellian moment, and we can write

$$M_n = M_n^M \eta^{\frac{n}{2}} \mathcal{W}(\eta, \zeta, \xi). \quad (17)$$

Thus, it is sufficient to discuss in the following only the normalized moments

$$\tilde{M}_n = \frac{M_n}{M^M} \quad (18)$$

and, analogously, for  $\tilde{v}_p$  and  $\tilde{P}$ , and for the distribution function  $\tilde{f}$ .

The recipes with  $\eta \neq 1$  or  $\xi \neq 1$  result in a scaling of the Maxwellian and can easily be obtained from the above, though, they will not be discussed further.

### 4.2 The $\xi = 0$ recipes

With the choice of  $\xi = 0$  the cutoff part vanishes and we are left with

$$\tilde{f}(\eta, \zeta, 0) = \frac{1}{\eta^{\frac{3}{2}}} \frac{\Gamma(\zeta)}{\Gamma\left(\zeta - \frac{3}{2}\right)} \left(1 + \frac{v^2}{\eta\Theta^2}\right)^{-\zeta}, \quad (19)$$

where we have used Eq. (A6). The moments are

$$\tilde{M}_n = \eta^{\frac{n}{2}} \frac{\Gamma\left(\zeta - \frac{3+n}{2}\right)}{\Gamma\left(\zeta - \frac{3}{2}\right)} \quad \text{only if} \quad \zeta > \frac{3+n}{2}. \quad (20)$$

If we check now for the contribution of particles beyond the speed of light, i.e., we calculate the relative pressure according to Scherer et al. (2019a), which is the ratio  $R$  of the total thermal pressure  $\tilde{P}$  and the relative pressure  $P'$ :

$$R = 1 - \frac{P'}{P} \quad (21)$$

with

$$P' = \int_0^w \tilde{f} v^4 dv, \quad (22)$$

where the integral is cut off at the upper boundary  $w$ . Thus, it is easy to check that the ratio  $R$  does not depend on  $\eta$ . Therefore, we only need to estimate the integral in dependence of, say  $\zeta_0$ , and get the contribution from superluminal particles for all distribution functions  $\tilde{f}(\eta, \zeta_0, 0)$ . In the literature the function  $\zeta$  is determined by  $\zeta = \kappa + 1$ , and hence the superluminal contribution for  $\eta = \kappa$  or  $\eta = \kappa - \frac{3}{2}$  is the same. We can also state that with increasing flatness parameter  $\zeta(\kappa) > \zeta_0(\kappa)$ ,  $\forall \kappa$  the contribution becomes lower than that for  $\zeta_0 = \kappa + 1$  or higher if  $\zeta(\kappa) > \zeta_0(\kappa)$ ,  $\forall \kappa$ .

Thus, the recipes with  $\xi = 0$  have to be checked for the contribution of superluminal particles, before they can be applied to physical considerations. In the case that  $\zeta = \kappa + 1$ , which is quite often used in literature (see the references in the introduction), one should not choose for sufficiently high values of  $\Theta$  too low values of  $\kappa$ , see the discussion in Scherer et al. (2019a).

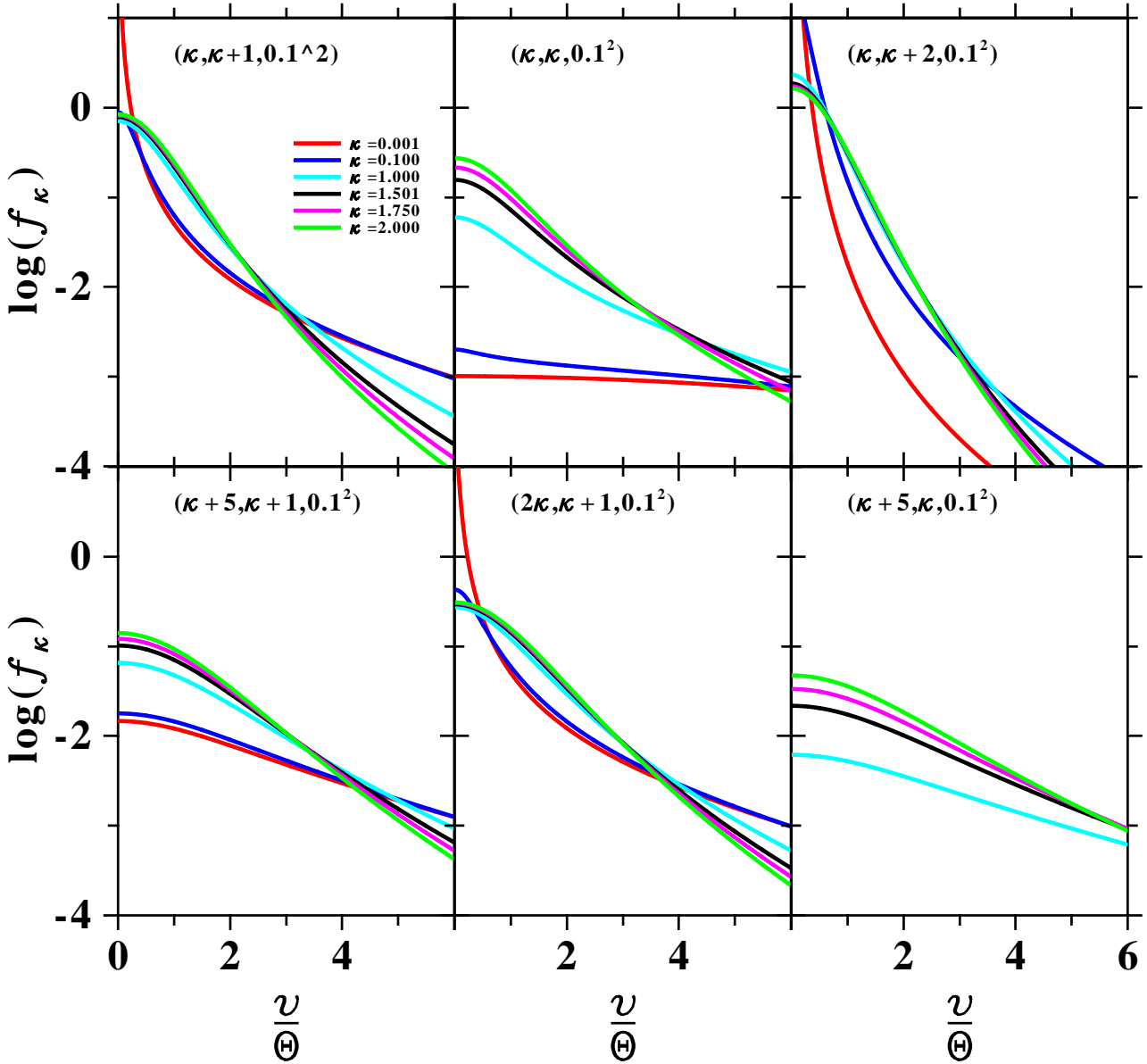


**Figure 1.** The shape and flatness parameters. The  $\kappa$  values can be found in the inlet of the left upper panel and are the same for all panels. For further discussion see main text.

### 4.3 $\eta = 0$ recipes

When this happens the distribution function from Eq. (3) goes to infinity for  $\kappa < \frac{3}{2}$ , or for  $\kappa > \frac{3}{2}$  to zero (see Appendix A4) and all moments vanish. Moreover, we see from Eq. (20) that the  $n$ th moment is proportional to  $\eta^{\frac{n}{2}}$  and therefore  $\eta$  should be strictly positive for non-vanishing moments. There is a special case when we require for a given moment, say the  $n$ th one,

$$\eta^{\frac{n}{2}} \frac{\Gamma(\zeta - \frac{3+n}{2})}{\Gamma(\zeta - \frac{3}{2})} = C, \quad (23)$$

where  $C$  is an arbitrary constant, which we can without loss of generality choose as  $C = 1$ , and if  $C \neq 1$  we divide  $\eta$  by  $C^{\frac{2}{n}}$ . Thus we have

$$\eta^{\frac{n}{2}} \Gamma\left(\zeta - \frac{3+n}{2}\right) = \Gamma\left(\zeta - \frac{3}{2}\right). \quad (24)$$

This equation can only hold when  $\Gamma(\zeta - \frac{3+n}{2})$  goes to (positive) infinity, because when  $\eta$  goes to zero, the right hand side of Eq. (24) is always positive. The first value at which the Gamma function on the left side goes to infinity is when  $\zeta = \frac{3+n}{2}$ . Inserting that value in the Gamma function on the right hand side leads to  $\Gamma(\frac{n}{2})$ . If we find now a solutions for  $\eta_1$  at  $n = n_1$ , it is evident that we cannot find other solution with  $n \neq n_1$ , because for another moment, say  $n_2$ , Eq. (24) has a different solution  $\eta_2$ , which is not possible, because for all moments  $\eta$  should be the same. Thus, we can find an  $n_1$  and  $\eta_1$  for which Eq. (24) is fulfilled when  $\eta_1 \rightarrow 0$ , but for all other  $n$  the moments  $\tilde{M}_{n \neq n_1} = 0$  vanish. That leads to a physically strange situation, where the moment  $\tilde{M}_{n=n_1} = 1$  is one and all others  $\tilde{M}_{n \neq n_1} = 0$  are zero. For example if  $n_1 = 2$ , the second moment (i.e., the pressure) is one ( $\tilde{M}_2 = \tilde{P} = 1$ ), but all other moments vanish when  $\eta_1 \rightarrow 0$ . That means we have a constant pressure (temperature) but a vanishing



$n$	$\zeta$	$\eta$
1	$\kappa$	$\left(\frac{\Gamma(\kappa-\frac{3}{2})}{\Gamma(\kappa-2)}\right)^2$
1	$\kappa+1$	$\left(\frac{\Gamma(\kappa-\frac{1}{2})}{\Gamma(\kappa-1)}\right)^2$
2	$\kappa$	$\kappa-\frac{5}{2}$
2	$\kappa+1$	$\kappa-\frac{3}{2}$

**Table 1.** Solutions of Eq. (25).

most probable speed for  $\eta_1 \rightarrow 0$ . Thus we have a gas with constant pressure but no internal motion, which is physically not meaningful.

The solution for  $\eta^{\frac{n}{2}}$  can easily be determined

$$\eta^{\frac{n}{2}} = \frac{\Gamma(\zeta - \frac{3}{2})}{\Gamma(\zeta - \frac{3+n}{2})}. \quad (25)$$

Some results for  $\zeta = \kappa$  and  $\zeta = \kappa+1$  are given in Table 1.

From Table 1 it becomes clear that the choice of  $\eta = \kappa - \frac{3}{2}$  comes from the requirement that the second moment for  $\zeta = \kappa+1$  is constant and the temperature is equal to the Maxwellian temperature ( $M_2 = P = M_2^M \tilde{M} = M_2^M$ ), which has the deficit that all other moments vanish.

Thus, to conclude the above discussion, the recipes with  $\xi = 0$  have a couple of problems concerning their physical properties. The reason is that when  $\eta \rightarrow 0$ , the distribution function have a singularity and all moments approach zero, except the one, which is arbitrarily chosen to be constant.

## 5 SOME COMMONLY USED EXAMPLES

We now discuss some recipes found in literature (see Table 2) or which were suggested during our discussions. In the following we will always use  $\zeta = \kappa+1$ . The discussed distribution functions below can always be obtained by the proper choice of  $\xi(\kappa)$  and  $\eta(\kappa)$  (see Table 2).

The complete definition of the distribution functions is given in Table 3, where we have split the distribution functions in a normalization part, which consists of a Maxwellian (second column) and a remaining  $\kappa$ -part (third column), and a distribution part, which contains a power (fourth column) and a (possible) cutoff term (fifth column). It can be seen from Table 3 that the Maxwellian part is the same for all distribution functions as already discussed above. The remaining normalization part in the third column is a function of  $\kappa$  and  $\xi$  via the reciprocal of the Kummer- $U$  function, which is only the case if an exponential part in the distribution exists (that is for all recipes  $(\eta, \zeta, \xi)$  where  $\xi \neq 0$ ).

The tail-part of the distribution given in the fourth column and the ‘‘exponential’’ cutoff in the fifth column describe the ‘‘form’’ of the distribution function. The last two higher-ranking columns give the range, which is defined in such a way that the distribution function is always in  $\mathbb{R}_+$ . For the recipe  $(\kappa, \kappa+1, 0)$  (SKD) it is in principle possible to have lower  $\kappa$  values than  $\frac{3}{2}$ , but then the pressure is not defined (see below). Therefore, we choose for the SKD also as the lower limit  $\kappa = \frac{3}{2}$ . Nevertheless, if we allow lower  $\kappa$  values in the SKD, we find that the lower limit is  $\kappa = \frac{1}{2}$  at which the

name	recipe			reference
	$\eta$	$\zeta$	$\xi$	
SKD	$\kappa$	$\kappa+1$	0	(e.g., Olbert 1968)
				(Vasyliunas & Siscoe 1976)
	$\kappa$	$\kappa+1$	0	(Yoon 2014, not discussed here)
	$\kappa - \frac{3}{2}$	$\kappa+1$	0	(Livadiotis & McComas 2013)
	$\kappa$	$\kappa+r$	0	(Treumann & Baumjohann 2014)
RKD	$\kappa$	$\kappa+1$	$\alpha^2$	(Scherer et al. 2017b)
	$\kappa - \frac{3}{2}$	$\kappa+1$	$\alpha^2$	private communication
	$\kappa$	$\kappa+1$	$\frac{\kappa\alpha^2}{\kappa-\frac{3}{2}}$	
	$\kappa - \frac{3}{2}$	$\kappa+1$	$\frac{\kappa\alpha^2}{\kappa-\frac{3}{2}}$	(DeStefano 2019)

**Table 2.** The recipes  $(\eta, \zeta, \xi)$  for the discussed distribution functions, where  $\alpha^2 = \xi$  is used to be compatible with our earlier notation.

distribution vanishes. Thus, lower limits for the SKD and for the recipes  $(\kappa - \frac{3}{2}, \kappa+1, 0)$ ,  $(\kappa - \frac{3}{2}, \kappa+1, \xi^2)$ ,  $(\kappa, \kappa+1, \frac{\kappa\xi^2}{\kappa-\frac{3}{2}})$ , are always at  $\kappa = \frac{3}{2}$ , and that for the RKD at  $\kappa = 0$ . At that limit the SKD has finite values depending on the velocity. All other distribution functions (including the RKD) go to infinity, when  $v = 0$  (column 6), while for  $v \neq 0$  (column 7) only the RKD is a function of the velocity, while all the other discussed recipes tend to zero. The eighth column gives the upper limits, when  $\kappa \rightarrow \infty$ . In this limit the recipes with  $\xi = \text{const.}$  or  $\xi = 0$  approach a Maxwellian type distribution, while the recipes with  $\xi \propto (\kappa - \frac{3}{2})^{-1}$  tend to zero. The upper limits are calculated using the integral of the 0th order moment to determine the normalization factors when  $\kappa \rightarrow \infty$ . The above recipes are described in Table 2 with the corresponding reference. For further use we will call all the recipes with  $\kappa - \frac{3}{2}$  dependency in one or more parameter the  $\Psi$ -distributions.

The range of the SKD could be extended to  $\kappa \in (\frac{1}{2} \dots \infty)$ , but then neither the most probable speed nor the pressure are defined. All of the above distributions go to infinity when first  $v \rightarrow 0$  and then  $\kappa \rightarrow \frac{3}{2}$ , or  $\kappa \rightarrow 0$  in the case of the RKD. Therefore, we calculated two limits for  $\kappa \rightarrow 0$ : one for  $v = 0$  and one for  $v \neq 0$ . The calculations of the limits for the Kummer- $U$  function are presented in Appendix A2.

The limits of the Kummer- $U$  function are discussed in Appendix A2. The calculation of the normalization factors given in columns 2 and 3 of Table 3 are given in the Appendix B. The Kummer- $U$  or Tricomi function  $U(\frac{n+3}{2}, \frac{n+3}{2} - \kappa, x)$  is for arbitrary  $x$  approximated as  $U(\frac{n+3}{2}, \frac{n+3}{2}, x)$  if  $\kappa \rightarrow 0$ , and as  $U(\frac{n+3}{2}, \frac{n}{2}, x)$  if  $\kappa \rightarrow \frac{3}{2}$ . These approximations are quite good for  $\kappa \ll 1$ , as can be seen in Fig. 2, where the non-approximated functions are plotted.

In Fig. 2 the distribution functions corresponding to six recipes are plotted for  $\xi = 0.1$ . For the RKD for  $\kappa$ -values of  $\kappa \in \{0.001, 0.1, 1.0, 1.501, 1.75, 2.0\}$  while for the other five distributions only the values  $\kappa \in \{1.501, 1.75, 2.0\}$  are pre-

recipe	Normalization		Distribution		lower Limit		upper Limit
	Maxwellian	$\kappa$	tail	cutoff	$\lim_{\substack{\kappa \rightarrow 0 \\ \nu=0}} =$	$\lim_{\substack{\kappa \rightarrow 0 \\ \nu \neq 0}} =$	$\lim_{\kappa \rightarrow \infty} =$
$(\eta, \zeta, \xi^2)$	$\frac{n_0}{\sqrt{\pi^3} \Theta^3}$	$\frac{1}{\eta^{\frac{3}{2}}(\kappa)} \mathbb{W}^{[0]}(\kappa, \zeta, \eta \xi)$	$\left(1 + \frac{\nu^2}{\eta(\kappa)\Theta^2}\right)^{-\zeta(\kappa)}$	$e^{-\xi(\kappa) \frac{\nu^2}{\Theta^2}}$	–	–	–
$(\kappa, \kappa+1, 0)$	$\frac{n_0}{\sqrt{\pi^3} \Theta^3}$	$\frac{\Gamma(\kappa)}{\sqrt{\kappa} \Gamma(\kappa - \frac{1}{2})}$	$\left(1 + \frac{\nu^2}{\kappa \Theta^2}\right)^{-\kappa-1}$		$\infty$	$\frac{n_0}{\sqrt{6\pi}} \left(1 + \frac{2}{3} \frac{\nu^2}{\Theta^2}\right)^{-\frac{3}{2}}$	$\frac{n_0}{\sqrt{\pi^3} \Theta^3} e^{-\frac{\nu^2}{\Theta^2}}$
$(\kappa, \kappa+1, \xi^2)$	$\frac{n_0}{\sqrt{\pi^3} \Theta^3}$	$\frac{1}{\kappa^{\frac{3}{2}}} \mathbb{W}^{[0]}(\kappa, \kappa+1, \xi^2)$	$\left(1 + \frac{\nu^2}{\kappa \Theta^2}\right)^{-\kappa-1}$	$e^{-\xi^2 \frac{\nu^2}{\Theta^2}}$	$\infty$	$\frac{1}{2} \frac{n_0 \xi}{\sqrt{\pi^3} \Theta^{\nu^2}} e^{-\xi^2 \frac{\nu^2}{\Theta^2}}$	$\frac{n_0 (\xi^2+1)^{\frac{3}{2}}}{\sqrt{\pi^3} \Theta^3} e^{-(1+\xi^2) \frac{\nu^2}{\Theta^2}}$
$(\kappa - \frac{3}{2}, \kappa+1, 0)$	$\frac{n_0}{\sqrt{\pi^3} \Theta^3}$	$\frac{\kappa \Gamma(\kappa)}{\Gamma(\kappa - \frac{1}{2}) (\kappa - \frac{3}{2})^{\frac{3}{2}}}$	$\left(1 + \frac{\nu^2}{(\kappa - \frac{3}{2}) \Theta^2}\right)^{-\kappa-1}$		$\infty$	0	$\frac{n_0}{\sqrt{\pi^3} \Theta^3} e^{-\frac{\nu^2}{\Theta^2}}$
$(\kappa - \frac{3}{2}, \kappa+1, \xi^2)$	$\frac{n_0}{\sqrt{\pi^3} \Theta^3}$	$\frac{1}{(\kappa - \frac{3}{2})^{\frac{3}{2}}} \mathbb{W}^{[0]}(\kappa - \frac{3}{2}, \kappa+1, \xi^2)$	$\left(1 + \frac{\nu^2}{(\kappa - \frac{3}{2}) \Theta^2}\right)^{-\kappa-1}$	$e^{-\xi^2 \frac{\nu^2}{\Theta^2}}$	$\infty$	0	$\frac{n_0 (\xi^2+1)^{\frac{3}{2}}}{\sqrt{\pi^3} \Theta^3} e^{-(1+\xi^2) \frac{\nu^2}{\Theta^2}}$
$(\kappa, \kappa+1, \frac{\kappa \xi^2}{\kappa - \frac{3}{2}})$	$\frac{n_0}{\sqrt{\pi^3} \Theta^3}$	$\frac{1}{\kappa^{\frac{3}{2}}} \mathbb{W}^{[0]}(\kappa, \kappa+1, \frac{\kappa \xi^2}{\kappa - \frac{3}{2}})$	$\left(1 + \frac{\nu^2}{\kappa \Theta^2}\right)^{-\kappa-1}$	$e^{-\frac{\kappa \xi^2 \nu^2}{(\kappa - \frac{3}{2}) \Theta^2}}$	$\infty$	0	$\frac{n_0 (\xi^2+1)^{\frac{3}{2}}}{\sqrt{\pi^3} \Theta^3} e^{-(1+\xi^2) \frac{\nu^2}{\Theta^2}}$
$(\kappa - \frac{3}{2}, \kappa+1, \frac{\kappa \xi^2}{\kappa - \frac{3}{2}})$	$\frac{n_0}{\sqrt{\pi^3} \Theta^3}$	$\frac{1}{(\kappa - \frac{3}{2})^{\frac{3}{2}}} \mathbb{W}^{[0]}(\kappa - \frac{3}{2}, \kappa+1, \frac{\kappa \xi^2}{\kappa - \frac{3}{2}})$	$\left(1 + \frac{\nu^2}{(\kappa - \frac{3}{2}) \Theta^2}\right)^{-\kappa-1}$	$e^{-\frac{\kappa \xi^2 \nu^2}{(\kappa - \frac{3}{2}) \Theta^2}}$	$\infty$	0	$\frac{n_0 (\xi^2+1)^{\frac{3}{2}}}{\sqrt{\pi^3} \Theta^3} e^{-(1+\xi^2) \frac{\nu^2}{\Theta^2}}$

**Table 3.** The regularized and quasi-regularized distribution function. The range for all distributions is assumed to be  $\kappa \in (\frac{3}{2} \dots \infty)$ , except for the RKD, in which case it goes from  $\kappa \in (0 \dots \infty)$ .

sented. In the upper panels the SKD, RKD and recipe  $(\kappa - \frac{3}{2}, \kappa+1, 0)$  are shown, while in the lower panels the recipes  $(\kappa - \frac{3}{2}, \kappa+1, \xi^2)$ ,  $(\kappa, \kappa+1, \frac{\kappa \xi^2}{\kappa - \frac{3}{2}})$ , and  $(\kappa - \frac{3}{2}, \kappa+1, \frac{\kappa \xi^2}{\kappa - \frac{3}{2}})$  are presented. It can be seen that the  $\Psi$ -distributions decrease much faster with increasing  $\frac{\nu}{\Theta}$  than the SKD and the RKD. For the limiting values ( $\kappa = \frac{3}{2}$  for the SKD and  $\Psi$  distributions, and  $\kappa = 0$  for the RKD) all distribution functions tend to infinity, when  $\nu \rightarrow 0$ , except the SKD, which has a finite value for  $\nu = 0$ . For sufficiently high  $\kappa$  values we find a regular behavior for all distribution functions. Also, the strange behavior for the recipes  $(\kappa, \kappa+1, \frac{\kappa \xi^2}{\kappa - \frac{3}{2}})$  and  $(\kappa - \frac{3}{2}, \kappa+1, \frac{\kappa \xi^2}{\kappa - \frac{3}{2}})$  can be seen when  $\kappa = 1.501$ : For  $\nu = 0$  these distributions tend to infinity, but for  $\nu \neq 0$  they rapidly decrease towards zero. This is the same behavior as shown in Table 3. Also the recipe  $(\kappa - \frac{3}{2}, \kappa+1, 0)$  and recipe  $(\kappa - \frac{3}{2}, \kappa+1, \xi^2)$  tend to zero for  $\nu \neq 0$ , but this decrease is much weaker for  $\kappa = 1.501$ . The reason for this different behavior is the exponential term in the recipes  $(\kappa, \kappa+1, \frac{\kappa \xi^2}{\kappa - \frac{3}{2}})$  and  $(\kappa - \frac{3}{2}, \kappa+1, \frac{\kappa \xi^2}{\kappa - \frac{3}{2}})$ , which goes quickly to zero, when in the exponential term  $\kappa \rightarrow \frac{3}{2}$ .

A few words to the RKD: For  $\kappa$ -values below  $\kappa = \frac{3}{2}$  the tails become flatter up to high ratios of  $\frac{\nu}{\Theta}$ . The tails for  $\kappa = 0.001$  and  $\kappa = 0.1$  are almost equal, while the latter has reasonable values at  $\nu \approx 0$ .

In Fig. 3 we changed the regularization parameter to  $\xi = 10^{-5}$ , which does not affect the SKD and recipe  $(\kappa - \frac{3}{2}, \kappa+1, 0)$ , but the other distributions. The recipe  $(\kappa - \frac{3}{2}, \kappa+1, \xi^2)$  and recipe  $(\kappa - \frac{3}{2}, \kappa+1, \frac{\kappa \xi^2}{\kappa - \frac{3}{2}})$  are more relaxed for low  $\kappa$ -values, because the low  $\xi$  cancels the steep cutoff at low values of  $\frac{\nu}{\Theta}$ , but will steeply fall off for high enough  $\kappa$ -values. The recipe  $(\kappa, \kappa+1, \frac{\kappa \xi^2}{\kappa - \frac{3}{2}})$  behaves similar to the SKD, but with a cutoff (not shown). The RKD has now for low  $\kappa$ -values lower finite values at  $\nu \approx 0$  and again flat tails for low  $\kappa$ -values. Also, for such low  $\xi$  values the recipes  $(\kappa - \frac{3}{2}, \kappa+1, \xi^2)$  and  $(\kappa - \frac{3}{2}, \kappa+1, \frac{\kappa \xi^2}{\kappa - \frac{3}{2}})$  fall faster towards zero than the SKD and the RKD (the recipe  $(\kappa - \frac{3}{2}, \kappa+1, 0)$  does also, but it depends not on  $\xi$ ).

One can also see, especially from Fig. 2 that for the RKD the Maxwellian core becomes lower, when the tails become flatter, i.e., the  $\kappa$ -values are low. This can be understood, because the number of particles is constant and thus, if there are more particles in the tail, less particles can be in the Maxwellian core.

## 6 HIGHER-ORDER MOMENTS

In Table 4 the higher-order moments, i.e., the most probable speed (1. moment) and the pressure (2. moment) are presented together with the Debye length. The corresponding integrals can be found in the Appendices B and C. The Debye length will be discussed separately in section 7.

Again, we find that the most probable speed and pressure can be decomposed into a Maxwellian part and a  $\kappa$ -dependent part. Thus, we will use the short hand notation:  $\tilde{u}_p = u_p \frac{\sqrt{\pi}}{2n_0\Theta}$  and  $\tilde{P} = P \frac{3}{2n_0\Theta^2}$ . This holds also true for the Debye length, which has a Maxwellian-like and a  $\kappa$ -part:  $\tilde{\Lambda}^2 = \Lambda^2 \frac{q^2 n_0}{\epsilon_0 m \Theta^2} = \frac{\Lambda^2}{\Lambda_0^2}$ , where  $\Lambda_0^2 = \frac{\epsilon_0 m \Theta^2}{q^2 n_0}$  is similar to the Maxwellian Debye length, except that the core speed  $\Theta$  is used instead of the Maxwellian thermal speed  $v_{th}$ . Here,  $q$  is the elementary charge,  $\epsilon_0$  the electric permittivity for vacuum, and  $m$  the particle mass in mind.

In Table 5 the lower and upper limits are given (for the Debye length see the discussion in Section 7). In Fig. 4 the non-Maxwellian part of the most probable speed  $\tilde{u}_p$  and in Fig. 5 that of the pressure  $\tilde{P}$  are plotted. From Table 4 we see that the most probable speed depends on either the square root of  $\kappa$  or  $\kappa - \frac{3}{2}$ , while the pressure is linearly dependent on  $\kappa$  or  $\kappa - \frac{3}{2}$ . Additionally, there are some factors which are specific to the underlying distribution function: for the SKD these are  $\Gamma$ -functions  $\left(\frac{1}{\kappa - \frac{3}{2}} = \frac{\Gamma(\kappa - \frac{3}{2})}{\Gamma(\kappa - \frac{1}{2})}\right)$ , while for the distributions with an exponential part these are Kummer- $U$  functions. An exception is the recipe  $(\kappa - \frac{3}{2}, \kappa+1, 0)$ , where the most probable speed depends also on  $\Gamma$ -functions, the pressure is constant, i.e., it does not depend on  $\kappa$ .

In Table 5 the lower and upper limits are given. One

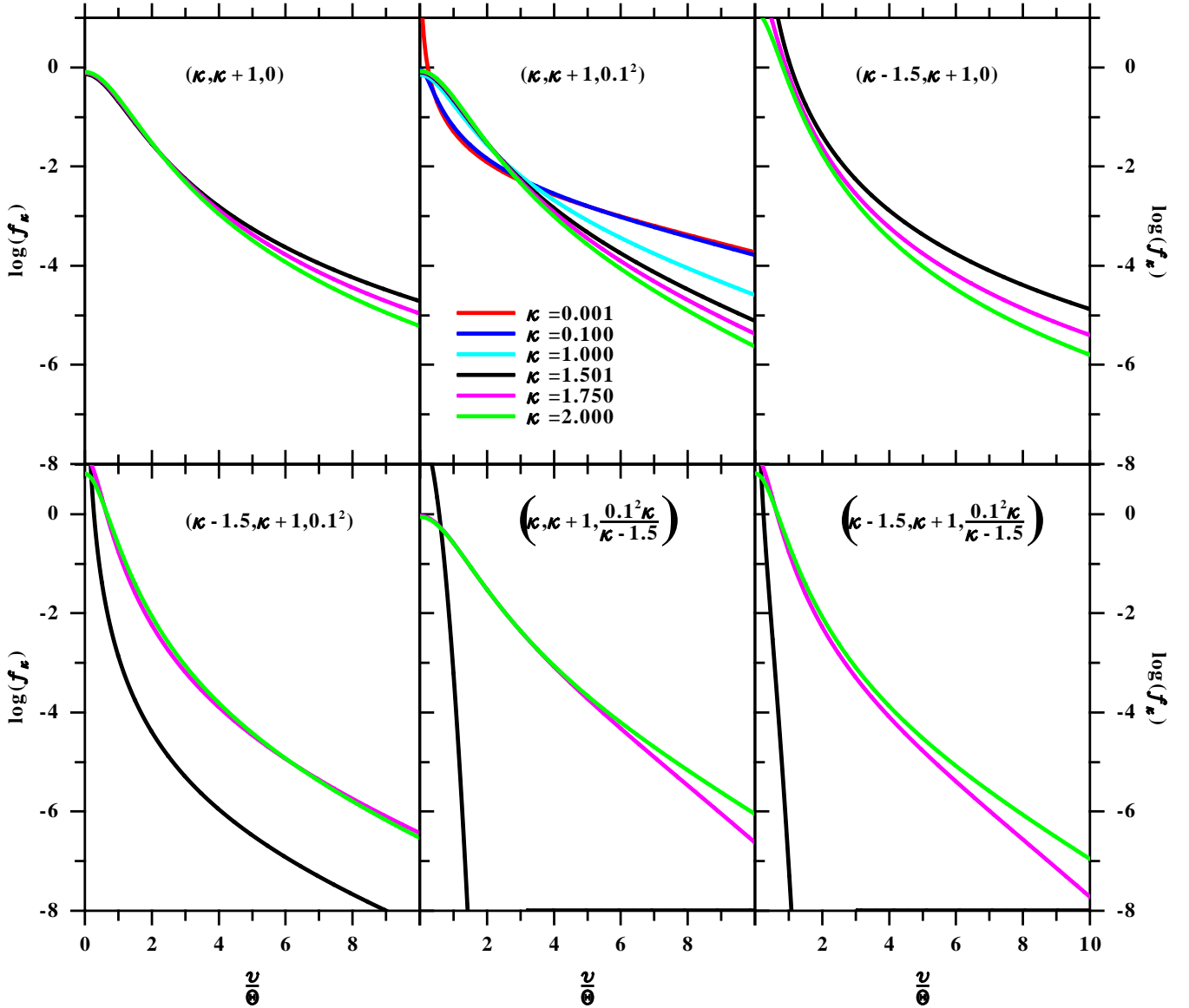


**Figure 2.** The different normalized distribution functions  $f_p$  for  $\xi = 10^{-1}$ . The color codes are the same for all six panels. Only for the recipe  $(\kappa, \kappa+1, \xi^2)$  (RKD) the first three  $\kappa$ -values are meaningful. It can be seen that only the recipes  $(\kappa, \kappa+1, 0)$  (SKD) and  $(\kappa, \kappa+1, \frac{\kappa\xi^2}{\kappa-\frac{3}{2}})$  have finite values when  $\kappa \rightarrow \frac{3}{2}$ , while the recipes  $(\kappa-\frac{3}{2}, \kappa+1, 0)$ ,  $(\kappa-\frac{3}{2}, \kappa+1, \xi^2)$ , and  $(\kappa-\frac{3}{2}, \kappa+1, \frac{\kappa\xi^2}{\kappa-\frac{3}{2}})$  go to infinity when  $\kappa \rightarrow \frac{3}{2}$ . The RKD is also defined for all values  $\kappa > 0$ . It can also be seen that the recipes  $(\kappa-\frac{3}{2}, \kappa+1, 0)$ ,  $(\kappa-\frac{3}{2}, \kappa+1, \xi^2)$ ,  $(\kappa, \kappa+1, \frac{\kappa\xi^2}{\kappa-\frac{3}{2}})$ , and  $(\kappa-\frac{3}{2}, \kappa+1, \frac{\kappa\xi^2}{\kappa-\frac{3}{2}})$  fall faster to zero with increasing  $\kappa$  than the SKD and RKD.

can see that only for the SKD and RKD the most probable speed has finite values when  $\kappa$  reaches its limit  $\kappa = \frac{3}{2}$ , for the  $\Psi$ -functions the most probable speed vanishes. The upper limits are for all distribution functions one or close to one.

A similar behavior can be seen for the pressure: The SKD goes to infinity when  $\kappa \rightarrow \frac{3}{2}$ , the RKD remains finite at a value  $1/(3\xi^2)$ , the recipe  $(\kappa-\frac{3}{2}, \kappa+1, 0)$  is constant, and the other three distributions go to zero. The upper limits are again one or close to one

The limits are evaluated with the help of Table A3 assuming that the second argument of the Kummer- $U$  function, i.e.,  $\frac{v+3}{2} - \kappa$  is for low  $\kappa$ -values in a very good approx-

imation  $\lim_{\kappa \rightarrow 0} \frac{v+3}{2} - \kappa = \frac{v+3}{2}$ , but the third argument  $\kappa\xi^2$  is still not zero. For  $\kappa \rightarrow \infty$  it is easiest to go back to the original integral expression, let first  $\kappa \rightarrow \infty$ , and then estimate the integrals.

From Table 4 and from Figs. 4 and 5 one can see that the most probable speed and pressures for the SKD and RKD behave as expected: The most probable speeds are proportional to  $\sqrt{\kappa}$  (and to those in the  $\Gamma$ -function) and are defined for the SKD for all  $\kappa \geq \frac{3}{2}$  and for the RKD for all  $\kappa \geq 0$ . In both cases the most probable speed is monotonically decreasing with increasing  $\kappa$ , see Fig. 4. The same holds true for the pressure, see Fig. 5



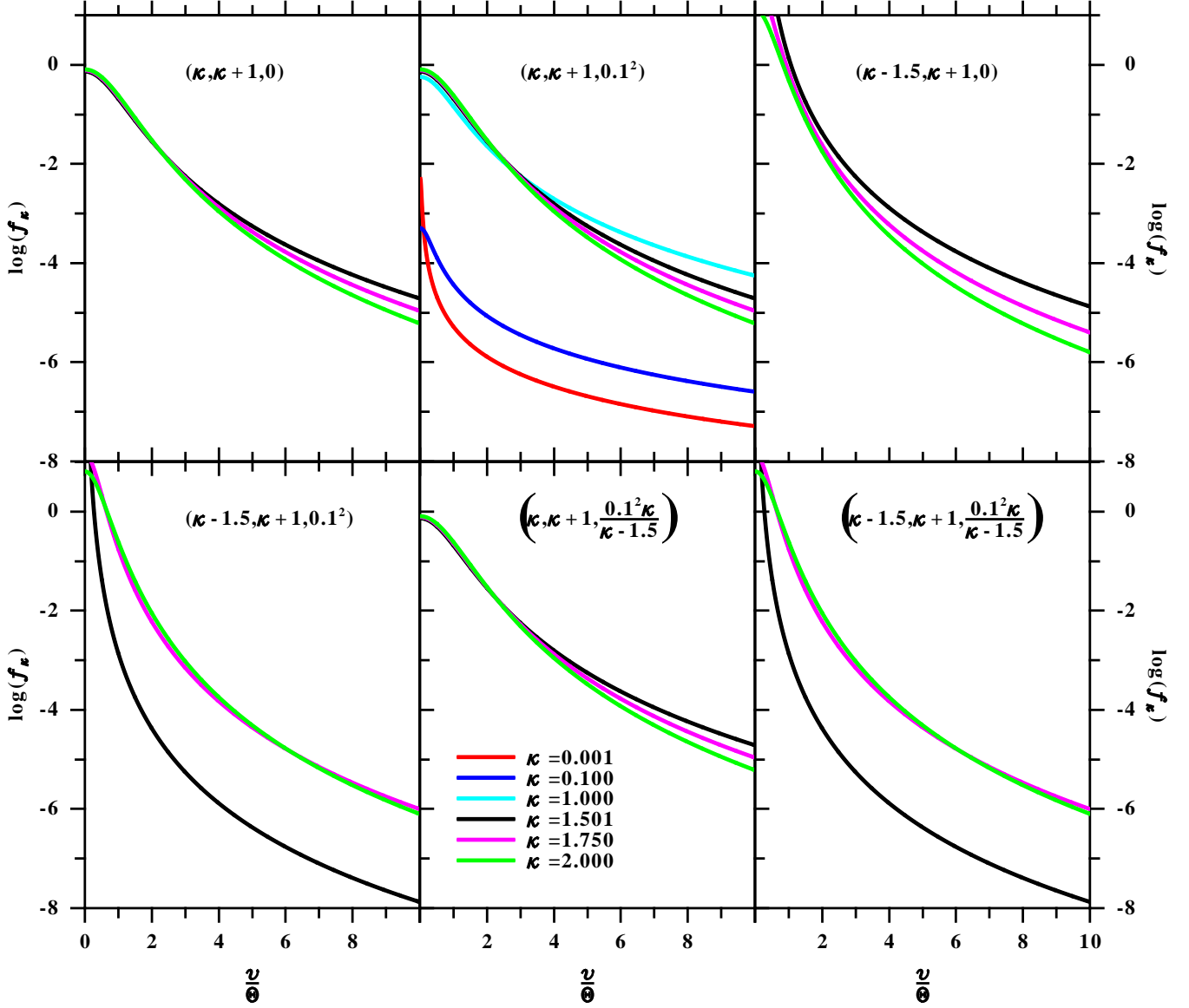


**Figure 3.** The different normalized distribution functions  $f_p$  for  $\xi = 10^{-5}$ . The colors are the same as in Fig. 2. It can be seen that the RKD has flatter tails for values  $\kappa < 1$ , but its absolute value is much below the  $\kappa > 1$ -values.

For the  $\Psi$ -distributions all speeds go to zero when  $\kappa \rightarrow \frac{3}{2}$ . The recipe  $(\kappa, \kappa + 1, \frac{\kappa \xi^2}{\kappa - \frac{3}{2}})$  distribution shows the best approximation to the SKD or RKD for higher  $\kappa$ -values, while the other  $\Psi$ -distributions (the recipes  $(\kappa - \frac{3}{2}, \kappa + 1, 0)$ ,  $(\kappa - \frac{3}{2}, \kappa + 1, \xi^2)$  and  $(\kappa - \frac{3}{2}, \kappa + 1, \frac{\kappa \xi^2}{\kappa - \frac{3}{2}})$ ) lie “much” below the reference curves of the SKD or RKD.

A similar behavior for the pressure can be seen in Fig. 5: by definition the recipe  $(\kappa - \frac{3}{2}, \kappa + 1, 0)$  pressure is constant (equal to the Maxwellian one), but for the recipes  $(\kappa - \frac{3}{2}, \kappa + 1, \xi^2)$ ,  $(\kappa, \kappa + 1, \frac{\kappa \xi^2}{\kappa - \frac{3}{2}})$  and  $(\kappa - \frac{3}{2}, \kappa + 1, \frac{\kappa \xi^2}{\kappa - \frac{3}{2}})$  distributions the pressure goes to zero when  $\kappa \rightarrow \frac{3}{2}$ . The SKD goes to infinity for  $\kappa \rightarrow \frac{3}{2}$ , while the RKD has a finite value for  $\kappa > 0$  depending also on  $\xi$ .

The higher-order moments behave similar (not shown): Except for the recipe  $(\kappa - \frac{3}{2}, \kappa + 1, 0)$ , the higher-order mo-

ments  $M_{n>2}$  for the  $\Psi$ -distributions approach zero with decreasing  $\kappa$ . The higher-order moments of the recipe  $(\kappa - \frac{3}{2}, \kappa + 1, 0)$  behave similar to the SKD and require higher  $\kappa$ -values to be defined ( $\kappa \geq \frac{n+1}{2}$ ).

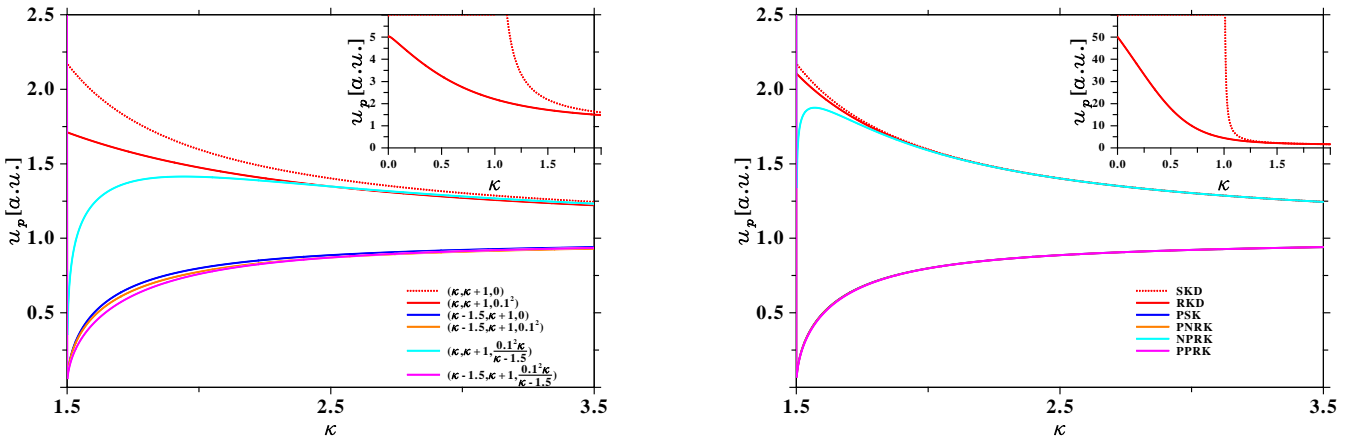
## 7 THE DEBYE LENGTH

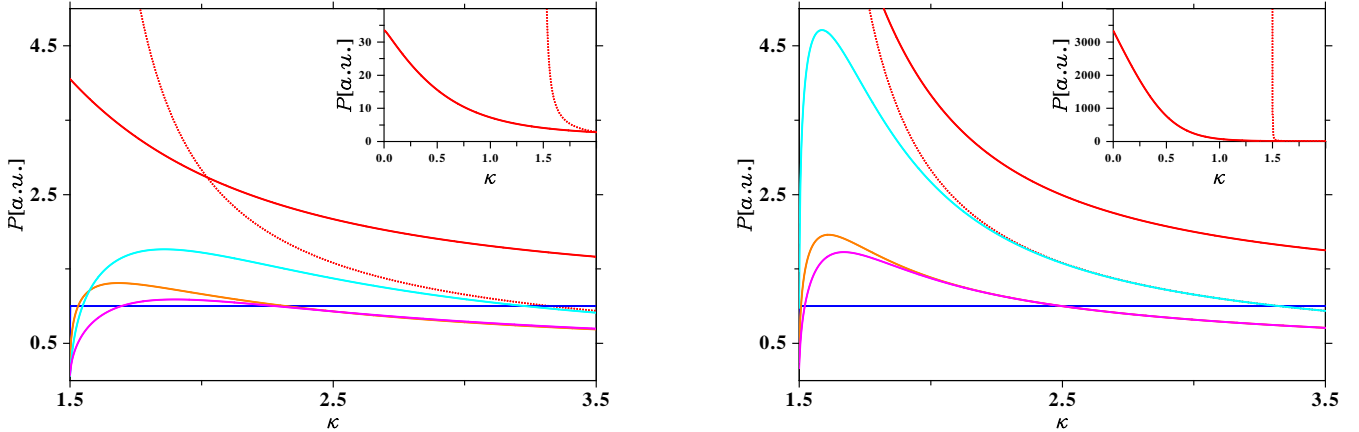
The Debye length is discussed in Treumann et al. (2004), Livadiotis & McComas (2004) and Fahr & Heyl (2016) as well as in Livadiotis et al. (2018, and references therein). These authors use the Debye-Hückel theory to determine the Debye length (see Appendix C). Because we are mainly dealing with collisionless plasmas, we apply here the approach discussed in (Krall & Trivelpiece 1973). In this approach a uniformly moving point test charge is considered to cause a small perturbation in a Vlasov plasma, which is otherwise

name	recipe	most probable Speed $u_p$		Pressure $P$		Debye length $\tilde{\Lambda}^2$		
		$\frac{2n_0}{\sqrt{\pi}}\Theta$	$\eta^{\frac{1}{2}}(\kappa)$	$^{[1]}\mathcal{W}^{[0]}(\eta, \zeta, \xi)$	$\frac{2n_0}{3}\Theta^2$	$\eta(\kappa)$	$^{[2]}\mathcal{W}^{[0]}(\eta, \zeta, \xi)$	$\left(\frac{\zeta}{\eta} \frac{U(\frac{3}{2}, \frac{3}{2}, \frac{3}{2}, \zeta, \eta\xi)}{U(\frac{3}{2}, \frac{3}{2}, \frac{3}{2}, \zeta, \eta\xi)} + \xi\right)^{-1}$
GKD	$(\eta, \zeta, \xi)$	$\frac{2n_0}{\sqrt{\pi}}\Theta$	$\eta^{\frac{1}{2}}(\kappa)$	$^{[1]}\mathcal{W}^{[0]}(\eta, \zeta, \xi)$	$\frac{2n_0}{3}\Theta^2$	$\eta(\kappa)$	$^{[2]}\mathcal{W}^{[0]}(\eta, \zeta, \xi)$	$\left(\frac{\zeta}{\eta} \frac{U(\frac{3}{2}, \frac{3}{2}, \frac{3}{2}, \zeta, \eta\xi)}{U(\frac{3}{2}, \frac{3}{2}, \frac{3}{2}, \zeta, \eta\xi)} + \xi\right)^{-1}$
SKD	$(\kappa, \kappa+1, 0)$	$\frac{2n_0}{\sqrt{\pi}}\Theta$	$\sqrt{\kappa}$	$\frac{\Gamma(\kappa-1)}{\Gamma(\kappa-\frac{1}{2})}$	$\frac{2n_0}{3}\Theta^2$	$\kappa$	$\frac{1}{\kappa-\frac{3}{2}}$	$\frac{\kappa}{\kappa-\frac{3}{2}}$
RKD	$(\kappa, \kappa+1, \xi^2)$	$\frac{2n_0}{\sqrt{\pi}}\Theta$	$\sqrt{\kappa}$	$^{[1]}\mathcal{W}^{[0]}(\kappa, \kappa+1, \xi^2)$	$\frac{2n_0}{3}\Theta^2$	$\kappa$	$^{[2]}\mathcal{W}^{[0]}(\kappa, \kappa+1, \xi^2)$	$\left[\frac{\kappa+1}{\kappa} \frac{U(\frac{3}{2}, \frac{3}{2}, \frac{3}{2}, \kappa, \kappa\xi^2)}{U(\frac{3}{2}, \frac{3}{2}, \frac{3}{2}, \kappa, \kappa\xi^2)} + \xi^2\right]^{-1}$
	$(\kappa-\frac{3}{2}, \kappa+1, 0)$	$\frac{2n_0}{\sqrt{\pi}}\Theta$	$(\kappa-\frac{3}{2})^{\frac{1}{2}}$	$\frac{\Gamma(\kappa-1)}{\Gamma(\kappa-\frac{1}{2})}$	$\frac{2n_0}{3}\Theta^2$	1	1	$\frac{\kappa-\frac{3}{2}}{\kappa-\frac{3}{2}}$
	$(\kappa-\frac{3}{2}, \kappa+1, \xi^2)$	$\frac{2n_0}{\sqrt{\pi}}\Theta$	$(\kappa-\frac{3}{2})^{\frac{1}{2}}$	$^{[1]}\mathcal{W}^{[0]}(\kappa-\frac{3}{2}, \kappa+1, \xi^2)$	$\frac{2n_0}{3}\Theta^2$	$(\kappa-\frac{3}{2})$	$^{[2]}\mathcal{W}^{[0]}(\kappa-\frac{3}{2}, \kappa+1, \xi^2)$	$\left[\frac{\kappa+1}{\kappa-\frac{3}{2}} \frac{U(\frac{3}{2}, \frac{3}{2}, \frac{3}{2}, \kappa-\frac{3}{2}, \xi^2)}{U(\frac{3}{2}, \frac{3}{2}, \frac{3}{2}, \kappa-\frac{3}{2}, \xi^2)} + \xi^2\right]^{-1}$
	$(\kappa, \kappa+1, \frac{\kappa\xi^2}{\kappa-\frac{3}{2}})$	$\frac{2n_0}{\sqrt{\pi}}\Theta$	$\sqrt{\kappa}$	$^{[1]}\mathcal{W}^{[0]}(\kappa, \kappa+1, \frac{\kappa\xi^2}{\kappa-\frac{3}{2}})$	$\frac{2n_0}{3}\Theta^2$	$\kappa$	$^{[2]}\mathcal{W}^{[0]}(\kappa, \kappa+1, \frac{\kappa\xi^2}{\kappa-\frac{3}{2}})$	$\left[\frac{\kappa+1}{\kappa} \frac{U(\frac{3}{2}, \frac{3}{2}, \frac{3}{2}, \kappa, \frac{\kappa\xi^2}{\kappa-\frac{3}{2}})}{U(\frac{3}{2}, \frac{3}{2}, \frac{3}{2}, \kappa, \frac{\kappa\xi^2}{\kappa-\frac{3}{2}})} + \frac{\kappa\xi^2}{\kappa-\frac{3}{2}}\right]^{-1}$
	$(\kappa-\frac{3}{2}, \kappa+1, \frac{\kappa\xi^2}{\kappa-\frac{3}{2}})$	$\frac{2n_0}{\sqrt{\pi}}\Theta$	$(\kappa-\frac{3}{2})^{\frac{1}{2}}$	$^{[1]}\mathcal{W}^{[0]}(\kappa-\frac{3}{2}, \kappa+1, \frac{\kappa\xi^2}{\kappa-\frac{3}{2}})$	$\frac{2n_0}{3}\Theta^2$	$(\kappa-\frac{3}{2})$	$^{[2]}\mathcal{W}^{[0]}(\kappa-\frac{3}{2}, \kappa+1, \frac{\kappa\xi^2}{\kappa-\frac{3}{2}})$	$\left[\frac{\kappa+1}{\kappa-\frac{3}{2}} \frac{U(\frac{3}{2}, \frac{3}{2}, \frac{3}{2}, \kappa-\frac{3}{2}, \frac{\kappa\xi^2}{\kappa-\frac{3}{2}})}{U(\frac{3}{2}, \frac{3}{2}, \frac{3}{2}, \kappa-\frac{3}{2}, \frac{\kappa\xi^2}{\kappa-\frac{3}{2}})} + \frac{\kappa\xi^2}{\kappa-\frac{3}{2}}\right]^{-1}$

**Table 4.** The most probable speeds, pressures and the normalized Debye lengths .

name	recipe	limit $\tilde{u}_p$		limit $\tilde{P}$		limit $\tilde{\Lambda}_D$	
		lower	upper	lower	upper	lower	upper
SKD	$(\kappa, \kappa+1, 0)$	$\lim_{\kappa \rightarrow \frac{3}{2}} \tilde{u}_p = \frac{\sqrt{6\pi}}{2}$	$\lim_{\kappa \rightarrow \infty} \tilde{u}_p = 1$	$\lim_{\kappa \rightarrow \frac{3}{2}} \tilde{P} = \infty$	$\lim_{\kappa \rightarrow \infty} \tilde{P} = 1$	$\lim_{\kappa \rightarrow \frac{3}{2}} \tilde{\Lambda}_D = \frac{2}{3}$	$\lim_{\kappa \rightarrow \infty} \tilde{\Lambda}_D = 1$
RKD	$(\kappa, \kappa+1, \xi^2)$	$\lim_{\kappa \rightarrow 0} \tilde{u}_p = \frac{1}{2\xi}$	$\lim_{\kappa \rightarrow \infty} \tilde{u}_p = \frac{1}{\sqrt{1+\xi^2}}$	$\lim_{\kappa \rightarrow 0} \tilde{P} = \frac{1}{3\xi^2}$	$\lim_{\kappa \rightarrow \infty} \tilde{P} = \frac{1}{1+\xi^2}$	$\lim_{\kappa \rightarrow 0} \tilde{\Lambda}_D = \frac{1}{1+\xi^2}$	$\lim_{\kappa \rightarrow \infty} \tilde{\Lambda}_D = \frac{1}{1+\xi^2}$
	$(\kappa-\frac{3}{2}, \kappa+1, 0)$	$\lim_{\kappa \rightarrow \frac{3}{2}} \tilde{u}_p = 0$	$\lim_{\kappa \rightarrow \infty} \tilde{u}_p = 1$	$\lim_{\kappa \rightarrow \frac{3}{2}} \tilde{P} = 1$	$\lim_{\kappa \rightarrow \infty} \tilde{P} = 1$	$\lim_{\kappa \rightarrow \frac{3}{2}} \tilde{\Lambda}_D = 0$	$\lim_{\kappa \rightarrow \infty} \tilde{\Lambda}_D = 1$
	$(\kappa-\frac{3}{2}, \kappa+1, \xi^2)$	$\lim_{\kappa \rightarrow \frac{3}{2}} \tilde{u}_p = 0$	$\lim_{\kappa \rightarrow \infty} \tilde{u}_p = \frac{1}{\sqrt{1+\xi^2}}$	$\lim_{\kappa \rightarrow \frac{3}{2}} \tilde{P} = 0$	$\lim_{\kappa \rightarrow \infty} \tilde{P} = \frac{1}{1+\xi^2}$	$\lim_{\kappa \rightarrow \frac{3}{2}} \tilde{\Lambda}_D = 0$	$\lim_{\kappa \rightarrow \infty} \tilde{\Lambda}_D = \frac{1}{1+\xi^2}$
	$(\kappa, \kappa+1, \frac{\kappa\xi^2}{\kappa-\frac{3}{2}})$	$\lim_{\kappa \rightarrow \frac{3}{2}} \tilde{u}_p = 0$	$\lim_{\kappa \rightarrow \infty} \tilde{u}_p = 1$	$\lim_{\kappa \rightarrow \frac{3}{2}} \tilde{P} = 0$	$\lim_{\kappa \rightarrow \infty} \tilde{P} = 1$	$\lim_{\kappa \rightarrow \frac{3}{2}} \tilde{\Lambda}_D = 0$	$\lim_{\kappa \rightarrow \infty} \tilde{\Lambda}_D = \infty$
	$(\kappa-\frac{3}{2}, \kappa+1, \frac{\kappa\xi^2}{\kappa-\frac{3}{2}})$	$\lim_{\kappa \rightarrow \frac{3}{2}} \tilde{u}_p = 0$	$\lim_{\kappa \rightarrow \infty} \tilde{u}_p = 1$	$\lim_{\kappa \rightarrow \frac{3}{2}} \tilde{P} = 0$	$\lim_{\kappa \rightarrow \infty} \tilde{P} = 1$	$\lim_{\kappa \rightarrow \frac{3}{2}} \tilde{\Lambda}_D = 0$	$\lim_{\kappa \rightarrow \infty} \tilde{\Lambda}_D = 1$

**Table 5.** The limits for the most probable speed, pressure and Debye lengths.

**Figure 4.** Most probable speed. The common factors given in Table 4 are neglected, i.e.,  $\frac{2n_0}{\sqrt{\pi}}\Theta$ . The left panel is for  $\xi = 0.1$  and the right panel for  $\xi = 0.01$ . The inlay shows the values for  $\kappa < 2$  for the RKD and SKD. There it can nicely be seen that the lower limit for the RKD is  $\frac{1}{2\xi}$ . It can also be seen that the most probable speed for the SKD has its pole at  $\kappa = 1$  (Scherer et al. 2019a).



**Figure 5.** The pressure. The common factors given in Table 4 are neglected, i.e.,  $\frac{2m_0}{3}\Theta^2$ . The left panel is for  $\xi = 0.1$  and the right panel for  $\xi = 0.01$ . The inset shows the values for  $\kappa < 2$  for the RKD and SKD. There it can nicely be seen that the lower limit for the RKD is  $\frac{1}{3\xi^2}$ .

uniform and field-free. By linearizing the plasma distribution function and performing a Fourier-Laplace transformation of the Vlasov equation, the potential in the plasma created by the test charge can be calculated, from which then the Debye length can be derived (see Appendix C1). For distributions, which have only a single factor depending on  $v$  like the Maxwellian, SKD, and recipe  $(\kappa - \frac{3}{2}, \kappa + 1, 0)$ , we obtain the same results in both approaches. But when we have two or more factors depending on  $v$ , like all the distributions with a cutoff, we get slightly different results.

We have derived the Debye length  $\Lambda$  for a single species in the appendix with a Maxwellian normalization factor

$$\Lambda_M^2 = 2 \frac{\epsilon_0 m_s \Theta_s^2}{q^2 n_s}, \quad (26)$$

which are given in Table 4 and their limits in Table 5 (to save writing we have dropped the index  $s$  in what follows). It can be seen from Table 5 that the lower limits  $\kappa \rightarrow \frac{3}{2}$  of the  $\Psi$ -distributions for the Debye length are always zero. In that case we do not have a plasma, because the plasma parameter  $N_p = \frac{4\pi}{3} n_0 \Lambda^3$  is then zero. For  $\kappa$ -values close to the limit that may be also the case for the RKD, which has always a finite Debye length, but the plasma parameter may be low. For  $\kappa \rightarrow \infty$  the discussed Debye length approaches that of the Maxwellian Debye length.

The Debye length for the RKD is shown in Fig. 6 for two  $\xi$ -values and those for the SKD and  $\Psi$ -distributions in Fig. 7. The latter are shifted by a small amount (see legend), because otherwise they would lie more or less on top of each other. For the RKD is can be seen from Fig. 6 that for all  $\xi$ -values the lower limit is close to that of the Maxwellian Debye length, which is also the case for the upper limit. In between, at low  $\kappa$ -values, the RKD has a maximum, which can be quite high for low  $\xi$ -values. The RKD and the SKD (Fig. 7) approach the Maxwellian limit from above, while the  $\Psi$ -distributions (except the recipe  $(\kappa, \kappa + 1, \frac{\kappa \xi^2}{\kappa - \frac{3}{2}})$ ) approach them from below. In all cases except that of recipe  $(\kappa, \kappa + 1, \frac{\kappa \xi^2}{\kappa - \frac{3}{2}})$ , if one is not too close to the lower  $\kappa$  limit, the Debye radius is close to that of the Maxwellian distribution. Furthermore, because the upper and lower limit for the RKD are equal, the expected extremum (maximum) can

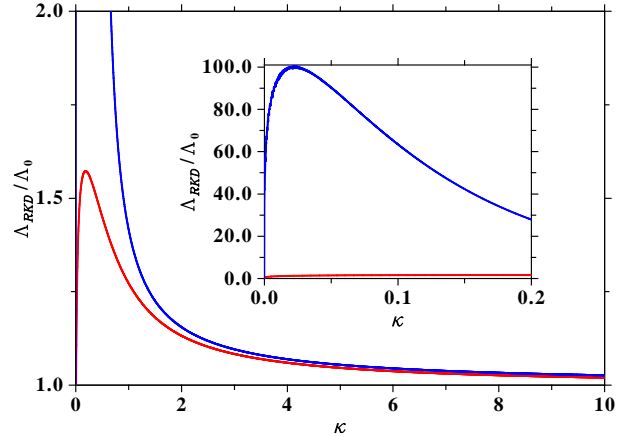


**Figure 6.** The Debye length  $\Lambda_{RKD}$  of the RKD normalized to that of the Maxwellian  $\Lambda_M$ . The red curves represent the case  $\xi = 0.1$ , while the blue curve shows  $\xi = 10^{-5}$ . It can be seen that both curves go in the limit  $\kappa \rightarrow 0$  to  $\frac{1}{1-\xi^2}$  and for  $\kappa \rightarrow \infty$  to the same limit. The maximum is at very low  $\kappa$ -values, and can be huge. Curves for  $10^{-5} \leq \xi \leq 10^{-1}$  lie between the above two limiting curves. It can be seen that at the maximum for  $\xi = 10^{-5}$  the numerics are not very good. The inset enlarges the view for low  $\kappa$  values.

clearly be seen. For low  $\xi$ -values it can be quite high, and drops quickly to the limit, when  $\kappa \rightarrow 0$ . The limit for  $\kappa \rightarrow \infty$  is not reached for the  $\kappa$ -values shown in Figs. 6 and 7.

Note: The Debye length  $\Lambda$  is a combination of the Debye lengths of all species. Thus, following Eq. (C4) we can also have the case that one species (say the electrons) is, for example,  $\kappa$ -distributed, while the other species (the ions) is Maxwellian distributed. Even if all species are  $\kappa$ -distributed it is very unlikely that both have the same  $\kappa$ -value. Moreover, by definition of a plasma the number of particles in a Debye sphere must be large, which is not the case when  $\Lambda \rightarrow 0$ , except when simultaneously the number density goes to infinity.

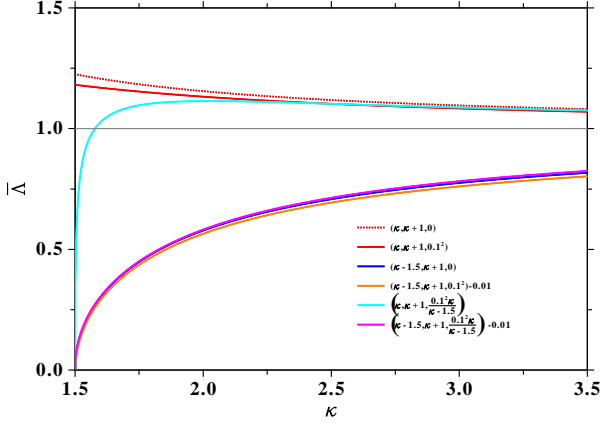


**Figure 7.** The Debye length for the  $\Psi$ -distributions and the SKD. It is obvious, that the  $\Psi$ -distributions, except the recipe  $(\kappa, \kappa + 1, \frac{\kappa^2}{\kappa - 1.5})$ , approach the upper limit from below, while the SKD from above.

## 8 APPLICATION TO OBSERVATIONS

### 8.1 Pressure and heat flow for a sum of distribution functions

To estimate the pressure and heat flow for the sum of distribution functions (Paschmann et al. 1998) is more complicated: It has to be taken in the center of mass system, which can be calculated as the first moment  $n\vec{u}$ :

$$\vec{u} = \frac{\sum_{i=1}^{i_{\max}} m_i n_i \vec{u}_i}{\sum_{i=1}^{i_{\max}} m_i n_i}, \quad (27)$$

where  $\vec{u}_i$  is the drift velocity of the species  $i$ ,  $n_i$  its number density and  $m_i$  its mass. With  $i_{\max}$  the total number of distribution functions involved is given. Thus the pressure is

$$\begin{aligned} \overleftrightarrow{P} &= \sum_{i=1}^{i_{\max}} m_i \int f_i(\vec{v} - \vec{u}_i) (\vec{v} - \vec{u}) \otimes (\vec{v} - \vec{u}) d^3v \\ &= \sum_{i=1}^{i_{\max}} m_i \int f_i(\vec{v}) (\vec{v} - \vec{u} + \vec{u}_i) \otimes (\vec{v} - \vec{u} + \vec{u}_i) d^3v \\ &= \sum_{i=1}^{i_{\max}} m_i \int f_i(\vec{v}) \left[ \underbrace{\vec{v} \otimes \vec{v}}_{\text{partial thermal pressure } \overleftrightarrow{P}_i} - \underbrace{(\vec{u} - \vec{u}_i) \otimes (\vec{u} - \vec{u}_i)}_{\text{internal ram pressure } \overleftrightarrow{R}_i} \right] d^3v, \end{aligned} \quad (28)$$

were we have neglected all the terms of the odd functional dependencies of  $\vec{v}$  and the double sided arrow over quantities denotes second-order tensors. The terms in the square brackets of Eq. (28) can be identified as the (isotropic) partial pressure tensor  $\overleftrightarrow{P}_i$  due to thermal motion, and the internal ram pressure tensor  $\overleftrightarrow{R}_i$  due to the bulk motion, each contributed by particle species  $i$ .

For isotropic distributions we are only interested in the trace of the pressure tensor ( $\vec{u}$  and  $\vec{u}_i$  (in Cartesian coordinates)):

$$\text{tr}(\overleftrightarrow{P}) = \sum_{i=1}^{i_{\max}} m_i \left( \text{tr}(\overleftrightarrow{P}_i) - \text{tr}(\overleftrightarrow{R}_i) \right)$$

$$= \sum_{i=1}^{i_{\max}} m_i \left( 3P_{11,i} - n_i (\vec{u} - \vec{u}_i)^2 \right). \quad (29)$$

For the heat flux the expression is much more complicated<sup>1</sup>:

$$\begin{aligned} \vec{H} &= \frac{1}{2} \sum_{i=1}^{i_{\max}} m_i \int f_i(\vec{v} - \vec{u}_i) (\vec{v} - \vec{u})^2 (\vec{v} - \vec{u}) d^3v \\ &= \frac{1}{2} \sum_{i=1}^{i_{\max}} m_i \int f_i(\vec{v}) (\vec{v} - \vec{u} + \vec{u}_i)^2 (\vec{v} - \vec{u} + \vec{u}_i) d^3v \\ &= \frac{1}{2} \sum_{i=1}^{i_{\max}} m_i \int f_i \left[ v^2 \vec{v} - 2(\vec{v} \cdot \vec{U}_i) \vec{v} + U_i^2 \vec{v} - v^2 \vec{U}_i + 2(\vec{v} \cdot \vec{U}_i) \vec{U}_i - U_i^2 \vec{U}_i \right] \\ &= \frac{1}{2} \sum_{i=1}^{i_{\max}} m_i \left( 2 \overleftrightarrow{P}_i + \text{tr}(\overleftrightarrow{P}_i) - n_i U_i^2 \right) \vec{U}_i \end{aligned} \quad (30)$$

with  $\vec{U}_i = \vec{u} - \vec{u}_i$ . The above pressure will be used in the following.

## 8.2 Fit to observations

### 8.2.1 High $\kappa$ -values

We demonstrate the use of the above discussed recipes using the electron data set from Ulysses, the event from 15.01.2002 at 3:33:42, which are shown in Fig. 8 for the parallel velocity component, i.e., only those parallel to the magnetic field. First, we assume that this is an ideal observed distribution function with no error bars. As discussed in Lazar et al. (2017), see also Maksimovic et al. (2005) and Štverák et al. (2008), these distributions  $f$  are best fitted by composite model distributions  $f(v) = f_c(v) + f_h(v) + f_s(v)$ , combining a quasithermal core (subscript  $c$ ) at low-energies, well reproduced by a standard Maxwellian, and two suprathermal components, the central halo (subscript  $h$ ) and the field-aligned strahl (subscript  $s$ ), each of them best fitted by Kappa power-laws. We may therefore reduce to a dual model

$$f = f_M(v, \Theta_M, u_M) + f_\kappa(v, \Theta_\kappa, u_\kappa), \quad (31)$$

where  $f_M$  is the Maxwellian core and  $f_\kappa$  incorporates the suprathermal (halo and strahl) populations. The recipes used for  $f_\kappa$  are indicated in the legends of Fig. 8. In a referential fixed to protons distribution functions may be assumed to depend not only on the velocity  $v$  and the core speed  $\Theta$ , but also on a drift (bulk) speed  $u$ . The non-linear fit is done in the following way: First we fit the Maxwellian part using only the values, which are in the  $3\sigma$  of the maximum value in the data set. These points are indicated by the red stars in the left panel of Fig. 8. The remaining data set is indicated by the black stars. In the next step we use these values as the starting point for the Maxwellian core in the combined distribution function, and then fit suprathermal tails, first with a SKD. The obtained fitted values are then used as reference for all the other recipes.

In the upper top panel of Fig. 8 the recipes are fitted. It can be seen that the fit approximates the right flank of the data better, compared to the left flank. That hints to an

<sup>1</sup> Eq. (30) is valid also for asymmetric distribution functions. In Eq.s (11) and (12) (as well as in the appendix Eq.s (B17) and (B20)) given by Scherer et al. (2019b) there are factors 2 missing.

Recipe	$n_M$ [cm <sup>-3</sup> ]	$\Theta_M$ [Mm <sup>-3</sup> ]	$u_M$ [Mm <sup>-3</sup> ]	$n_\kappa$ [cm <sup>-3</sup> ]	$\Theta_\kappa$ [Mm <sup>-3</sup> ]	$u_\kappa$ [Mm <sup>-3</sup> ]	$\eta$	$\zeta$	$\xi$	$a$	$b$	$c$	$d$
							$\kappa$	$\xi$	$\xi$				
(1,0,1)	0.505	1.227	0.054										
(1,0,1) + ( $\kappa, \kappa + 1, 0$ )	0.505	1.238	0.054	0.027	2.180	0.182	3.267	0.000E+00					
(1,0,1) + ( $\kappa, \kappa + 1, \xi^2$ )	0.507	1.234	0.054	0.025	2.159	0.167	3.411	0.523E-01					
(1,0,1) + ( $\kappa - 1.5, \kappa + 1, 0$ )	0.553	1.278	0.060	0.027	2.282	0.178	3.473	0.565E-01					
(1,0,1) + ( $\kappa - 1.5, \kappa + 1, \xi^2$ )	0.507	1.236	0.054	0.025	2.162	0.168	3.412	0.524E-01					
(1,0,1) + ( $\kappa, \kappa + 1, \xi^2 \kappa / (\kappa - 1.5)$ )	0.507	1.236	0.054	0.025	2.161	0.168	3.413	0.523E-01					
(1,0,1) + ( $\kappa - 1.5, \kappa + 1, \xi^2 \kappa / (\kappa - 1.5)$ )	0.507	1.236	0.054	0.025	2.160	0.168	3.414	0.523E-01					
(1,0,1) + ( $a \cdot \kappa + b, \kappa + 1, \xi^2$ )	0.508	1.235	0.054	0.025	2.162	0.168	3.418	0.524E-01	1.677	1.501	0.000	0.000	
(1,0,1) + ( $\kappa, c \cdot \kappa + d, \xi^2$ )	0.507	1.236	0.054	0.025	2.159	0.168	3.417	0.524E-01			1.015	1.549	
(1,0,1) + ( $a \cdot \kappa + b, c \cdot \kappa + d, \xi^2$ )	0.507	1.235	0.054	0.025	2.161	0.168	3.417	0.523E-01	1.601	0.850	1.375	0.866	
(1,0,1) + ( $\eta, \zeta, \xi^2$ )	0.508	1.235	0.054	0.025	2.159	0.168	3.414	4.160	0.524E-01				
< • >	0.511	1.239	0.055	0.026	2.176	0.170	3.405	0.470E-01					
$\sigma(\bullet)$	0.140E-01	0.131E-01	0.160E-02	0.811E-02	0.689E+00	0.054	1.078	0.217E-01					

**Table 6.** The number densities  $n_M, n_\kappa$ , core speeds  $\Theta_M, \Theta_\kappa$  and drift speeds  $u_M, u_\kappa$  for the Maxwellian part  $M$  and the  $\kappa$  recipes. The latter are given in the first column. The last two rows give the mean values and standard deviation for the corresponding column. See text for further discussion

Recipe	$u_{p,M}$ [km/s]	$P_M$ [m <sup>-1</sup> s <sup>-1</sup> ]	$R_M$ [m <sup>-1</sup> s <sup>-1</sup> ]	$u_{p,\kappa}$ [km/s]	$P_\kappa$ [m <sup>-1</sup> s <sup>-1</sup> ]	$R_\kappa$ [m <sup>-1</sup> s <sup>-1</sup> ]
(1,0,1)	699.4	0.507	0.0015	0.0	0.000	0.0000
(1,0,1) + ( $\kappa, \kappa + 1, 0$ )	706.3	0.517	0.0015	84.9	0.159	0.0009
(1,0,1) + ( $\kappa, \kappa + 1, \xi^2$ )	705.5	0.514	0.0015	70.4	0.085	0.0007
(1,0,1) + ( $\kappa - 1.5, \kappa + 1, 0$ )	797.9	0.602	0.0020	65.3	0.094	0.0009
(1,0,1) + ( $\kappa - 1.5, \kappa + 1, \xi^2$ )	706.8	0.516	0.0015	0.0	0.000	0.0007
(1,0,1) + ( $\kappa, \kappa + 1, \xi^2 \kappa / (\kappa - 1.5)$ )	707.4	0.517	0.0015	0.0	0.000	0.0007
(1,0,1) + ( $\kappa - 1.5, \kappa + 1, \xi^2 \kappa / (\kappa - 1.5)$ )	707.1	0.516	0.0015	0.0	0.000	0.0007
(1,0,1) + ( $a \cdot \kappa + b, \kappa + 1, \xi^2$ )	707.4	0.516	0.0015	66.0	0.065	0.0007
(1,0,1) + ( $\kappa, c \cdot \kappa + d, \xi^2$ )	707.7	0.517	0.0015	63.9	0.073	0.0007
(1,0,1) + ( $a \cdot \kappa + b, c \cdot \kappa + d, \xi^2$ )	707.2	0.516	0.0015	57.3	0.055	0.0007
(1,0,1) + ( $\eta, \zeta, \xi^2$ )	707.1	0.516	0.0015	73.8	0.091	0.0007
< • >	714.5	0.523	0.0015	43.8	0.057	0.0007
$\sigma(\bullet)$	26.4	0.025	0.0001	33.7	0.050	0.0002

**Table 7.** For the above recipes (also first column) the most probable speed, the thermal pressure and the ram pressure are presented. To get physical units, the pressure terms must be multiplied by the mass. The last two rows give the mean values and standard deviations for the corresponding column. See text for further information.

asymmetry or to the missing (explicit) fit for an additional "strahl"-component. Nevertheless, all discussed recipes lead to similar results concerning the fitted parameters, which are given in Table 6. In the last two rows of this table we present the mean value and the variance of corresponding parameters given by the discussed recipes. Although fits of some recipes may show deviations from the observations, it turns out that all the fitted functions lead to quite similar results with a quite small variance.

We can compare with plasma parameters provided by complementary measurements<sup>2</sup> at the time of observation of the above distribution function, e.g., the average solar

wind speed was  $u_{sw} = 636.3$  km/s with a temperature of  $T_{sw} = 104,599$  K and a proton number density of  $n_p = 0.22$  cm<sup>-3</sup> and a magnetic field strength of  $B = 0.75$  nT. The latter gives an Alfvén speed  $v_A = 35.6$  km/s.

Thus, the electron number density is by a factor 2 too high to guarantee charge neutrality. This is caused because we fit a spherical distribution function instead an anisotropic one to the data. If we assume that the maximum values of both distribution functions are equal, we find that the perpendicular must be of the order of 0.66 Mm. The average thermal speed of the core (Maxwellian) component  $\Theta_M$  is in a very good agreement with the electron sound speed  $c_e = 1.266$  Mm/s, while the average drift speed of the core is about the Alfvén speed. For the suprathermal component in the distribution function the average number density is

<sup>2</sup> taken from <https://omniweb.gsfc.nasa.gov/>



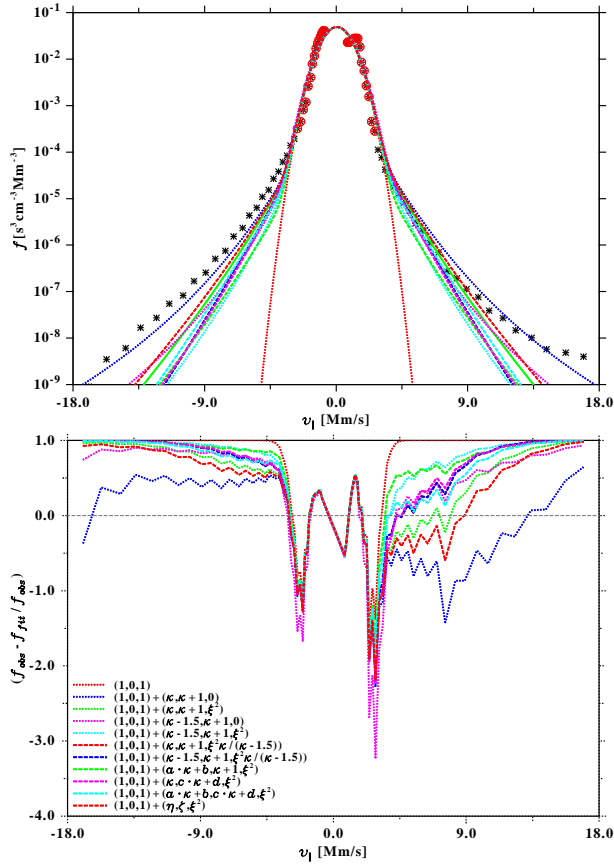


**Figure 8.** Top panel: The stars mark the Ulysses observations of the parallel part of an electron distribution. The recipes fitted are given in the legend. Bottom panel: The relative errors of recipes. See main text for more information.

roughly an order of magnitude less than the corresponding Maxwellian, but the average thermal speed is above twice that of Maxwellian core, and the average drift speed is three times higher than the core drift (see Table 6). Beside that the fits of the different recipes may not be that good, the above results show that all the discussed distribution functions lead to very similar macroscopic parameters like density, thermal and drift speeds.

The next criteria are the physical parameters, namely, the most probable speeds  $u_M$  or  $u_\kappa$ , the thermal pressures  $P_M$  and  $P_\kappa$  and the ram pressure  $R_M$  and  $R_\kappa$ . These values are calculated using Eq. (6). The results are presented in Tab 7. These parameters are also quite independent of the choice of the recipe. Also, the  $\kappa$ -values are all in the order of  $\kappa = 3$ . Thus, there is also no reason to discard one or the other discussed recipe, though the RKD-like models may present indubitable advantages (Scherer et al. 2017b, 2019b,a).

### 8.2.2 Low $\kappa$ -values

We present another data set from Ulysses (from 19.01.2002 at 08:19:49) where the  $\kappa$ -value is quite low ( $\kappa \approx 1.54$ ). The fit to the data is shown in the top panel of Fig. 9, while in the bottom panel the relative error is presented. Fits are in general much better than the previous one. We did not fit the recipes with  $\xi = 0$  because at such low  $\kappa$ -values the

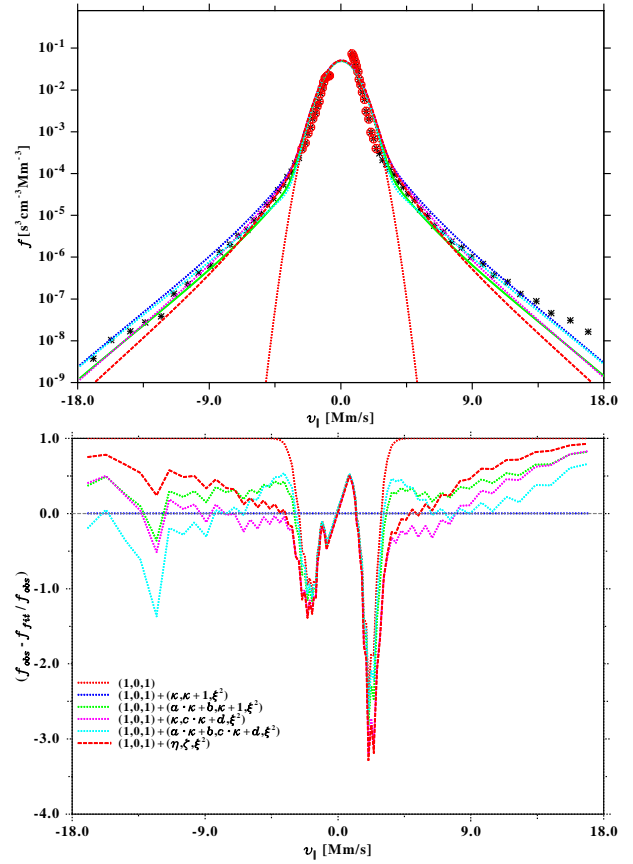


**Figure 9.** Top panel: The stars mark the Ulysses observations of the parallel part of an electron distribution. The recipes fitted are given in the legend. Bottom panel: The relative errors of recipes. See main text for more information.

contribution of superluminal particles to the pressure is not negligible (Scherer et al. 2019a). We have also neglected the recipes labeled with  $\kappa - 1.5$ , because of the most probable speed and all the moments which become indefinite when  $\kappa \rightarrow \frac{3}{2}$ . Remarkable is in this case the benefit of using RKD-like models, and, nevertheless, the remaining recipes give all similar macroscopic quantities, thus one can also use them to fit the data.

### 8.2.3 Conclusion from the fits

From the above fits one can conclude that all these fits of isotropic distribution functions (recipes) lead to very similar macroscopic parameters, excepting those which constrain the existence of these parameters (moments of order  $l$ ) only for sufficiently large values of  $\kappa (> (l+1)/2)$ . The “bad” fits to the data points indicate that the choice of an isotropic distribution function is not sufficient, but anisotropic or more detailed distribution functions, (e.g., separate halo and strahl) may offer more accurate descriptions. Also, the unrealistically high values obtained for the electron number density may have similar explanations. With 2D data sets, like those used here above, it becomes then possible to extend our present cookbook, by including anisotropic recipes, which we intend to write in the future.

Recipe	$n_M$ [cm $^{-3}$ ]	$\Theta_M$ [Mm $^{-3}$ ]	$u_M$ [Mm $^{-3}$ ]	$n_\kappa$ [cm $^{-3}$ ]	$\Theta_\kappa$ [Mm $^{-3}$ ]	$u_\kappa$ [Mm $^{-3}$ ]	$\eta$	$\zeta$	$\xi$	$a$	$b$	$c$	$d$
						$\kappa$		$\xi$					
(1,0,1)	0.505	1.227	0.054										
(1,0,1) + ( $\kappa, \kappa+1, \xi^2$ )	0.507	1.234	0.054	0.100	2.159	0.167		1.546	0.523E-01				
(1,0,1) + ( $a \cdot \kappa + b, \kappa+1, \xi^2$ )	0.508	1.235	0.054	0.100	2.162	0.168		1.547	0.524E-01	1.031	1.120		0.000
(1,0,1) + ( $\kappa, c \cdot \kappa + d, \xi^2$ )	0.507	1.235	0.054	0.100	2.163	0.168		1.549	0.523E-01			1.103	1.114
(1,0,1) + ( $a \cdot \kappa + b, c \cdot \kappa + d, \xi^2$ )	0.507	1.235	0.054	0.100	2.163	0.168		1.547	0.523E-01	1.720	0.820	1.255	0.570
(1,0,1) + ( $\eta, \zeta, \xi^2$ )	0.508	1.237	0.054	0.100	2.164	0.168	1.548	3.114	0.524E-01				
< $\bullet$ >	0.507	1.233	0.054	0.100	2.162	0.168		1.547	0.523E-01				
$\sigma(\bullet)$	0.854E-03	0.300E-02	0.170E-03	0.511E-04	0.135E-02	0.000		0.001	0.277E-04				

**Table 8.** Similar to Table 6 for the parallel data from day 19.01.2002 at 08:19:49. Here all the recipes with  $\xi = 0$  and containing the factor  $\kappa - \frac{3}{2}$  are neglected because of the low  $\kappa$  value. See text.

Recipe	$u_{p,M}$ [km/s]	$P_M$ [m $^{-1}$ s $^{-1}$ ]	$R_M$ [m $^{-1}$ s $^{-1}$ ]	$u_{p,\kappa}$ [km/s]	$P_\kappa$ [m $^{-1}$ s $^{-1}$ ]	$R_\kappa$ [m $^{-1}$ s $^{-1}$ ]
(1,0,1)	699.4	0.507	0.0015			
(1,0,1) + ( $\kappa, \kappa+1, \xi^2$ )	705.5	0.514	0.0015	336.9	0.592	0.0028
(1,0,1) + ( $a \cdot \kappa + b, \kappa+1, \xi^2$ )	707.3	0.516	0.0015	307.8	0.465	0.0028
(1,0,1) + ( $\kappa, c \cdot \kappa + d, \xi^2$ )	706.6	0.516	0.0015	304.1	0.493	0.0028
(1,0,1) + ( $a \cdot \kappa + b, c \cdot \kappa + d, \xi^2$ )	706.3	0.515	0.0015	297.2	0.422	0.0028
(1,0,1) + ( $\eta, \zeta, \xi^2$ )	708.2	0.517	0.0015	275.2	0.410	0.0028
< $\bullet$ >	705.5	0.514	0.0015	253.5	0.397	0.0023
$\sigma(\bullet)$	2.9	0.003	0.0000	114.8	0.187	0.0011

**Table 9.** Similar to Table 9 for the data set from the Ulysses data set at 19.01.2002 at 08:19:49. presented. See text for further discussion.

## 9 DISCUSSION AND CONCLUSION

In this paper we have presented a generalization of the  $\kappa$ -distributions, called the  $\kappa$ -cookbook, which unifies the various  $\kappa$ -distributions known in literature, called recipes. After laying out the required conditions for all distributions, we presented the generalized  $\kappa$ -distribution (GKD), and discussed its general properties and shape. Special cases with one of the parameters of the GKD being zero were discussed, and some commonly used  $\kappa$ -distributions were examined with respect to their limits and shape. Subsequently, we presented higher-order moments, i.e., the most probable speed (1. moment) and the pressure (2. moment) for the GKD and commonly used recipes, discussed the Debye length, and, ultimately, applied the examined recipes to fit real data measured by Ulysess.

The vanishing of the most probable speeds, the pressure (except for the recipe ( $\kappa - \frac{3}{2}, \kappa + 1, 0$ )) and Debye lengths for the recipes with  $\eta = \kappa \rightarrow \frac{3}{2}$  contradicts the physical interpretation that the distributions for rarefied gases “far” from equilibrium do have high most probable speeds or pressure like the SKD and RKD.

Even worse is the recipe ( $\kappa - \frac{3}{2}, \kappa + 1, 0$ ), because here we have a constant pressure, but a vanishing most probable speed for  $\kappa \rightarrow \frac{3}{2}$ . That means that the recipe ( $\kappa - \frac{3}{2}, \kappa + 1, 0$ ) has a finite pressure value, but no average speed. That behavior can be expected in a crystal at low temperatures, but not in a (rarefied) gas or plasma.

The recipe ( $\kappa - \frac{3}{2}, \kappa + 1, 0$ ) and SKD have the same problem concerning higher-order moments: the critical  $\kappa$ -value must increase with the order to get a finite moment, e.g.,

for the third moment  $\kappa > 2$  is required. The higher-order moments for the recipes with  $\eta = \kappa - \frac{3}{2}$  vanish when  $\kappa \rightarrow \frac{3}{2}$ , and thus these recipes with values close to that have problems, especially when  $\xi = 0$ , because then the contribution from superluminal particles becomes too large.

Let us assume that we have two distributions, one Maxwellian and another one constant. For the Maxwellian all moments exist, and for the constant distribution they are divergent or indefinite (do not exist). Thus, a general distribution with high-energy tails but Maxwellian core should have higher-order moments than the Maxwellian, because for lower  $\kappa$ -values the form part approaches a constant, but the distribution function becomes indefinite due to the normalization. With increasing  $\kappa$  the tails becomes steeper and the moments decrease and reach that of a Maxwellian.

It becomes thus clear that the RKD provides a practical alternative recipe for defining macroscopic moments of the observed distributions without any constraint for the power-law exponent  $\kappa$ . Our final result shows that all discussed recipes lead to similar macroscopic velocity moments, providing quantities like number density, core and drift speeds. Therefore, fitting the observed data with one of the above kappa recipes will not change the macroscopic behavior of the plasma and thus we have not to care about large scale fluid models (of the heliosphere), because they are all similar for the discussed distribution functions. Nevertheless, the microscopic (kinetic) behavior is affected by the choice of a recipe (Yoon et al. 2019; Husidic et al. 2020). Now when defining a new recipe, say, to better fit the data, it is easy with the above derived formulas to calculate the

velocity moments, Debye length etc. and compare them with the standard recipes for the SKD or RKD.

## 10 DATA AVAILABILITY STATEMENT

The datasets were derived from sources in the public domain: <https://omniweb.gsfc.nasa.gov/>

## REFERENCES

- Abramowitz M., Stegun I. A., 1972, *Handbook of Mathematical Functions*. Dover
- Balescu R., 1988, *Transport Processes in Plasmas*. North-Holland, <https://books.google.de/books?id=2BecSAAACAAJ>
- Davelaar J., Mościbrodzka M., Bronzwaer T., Falcke H., 2018, *Astron. Astrophys.*, 612, A34
- DeStefano A. M., 2019, PhD thesis, The University of Alabama in Huntsville
- Desai M. I., et al., 2012, *ApJ*, 749, L30
- Elkamash I. S., Kourakis I., 2016, *Phys. Rev. E*, 94, 053202
- Fahr H. J., Heyl M., 2016, *A&A*, 589
- Fahr H.-J., Sylla A., Fichtner H., Scherer K., 2016, *Journal of Geophysical Research (Space Physics)*, 121, 8203
- Fahr H.-J., Krimigis S. M., Fichtner H., Scherer K., Sylla A., Ferreira S. E. S., Potgieter M. S., 2017, *Astrophys. J. Lett.*, 848, L3
- Fichtner H., Scherer K., Lazar M., Fahr H. J., Vörös Z., 2018, *Phys. Rev. E*, 98, 053205
- Goedbloed J. P., Keppens R., Poedts S., 2010, *Advanced Magnetohydrodynamics*. Cambridge, UK: Cambridge University Press
- Hasegawa A., Mima K., Duong-van M., 1985, *Phys. Rev. Lett.*, 54, 2608
- Heerikhuisen J., Zirnstein E., Pogorelov N., 2015, *Journal of Geophysical Research (Space Physics)*, 120, 1516
- Heerikhuisen J., Zirnstein E. J., Pogorelov N. V., Zank G. P., Desai M., 2019, *ApJ*, 874, 76
- Husidic E., Lazar M., Fichtner H., Scherer K., Astfalk P., 2020, *Phys. Plasmas*, 27, 042110
- Krall N. A., Trivelpiece A. W., 1973, *Principles of plasma physics*. McGraw-Hill Book Company
- Lazar M., Poedts S., Fichtner H., 2015, *A&A*, 582, A124
- Lazar M., Pierrard V., Shaaban S. M., Fichtner H., Poedts S., 2017, *A&A*, 602, A44
- Lazar M., Scherer K., Fichtner H., Pierrard V., 2019, *A&A*, 634, A20
- Livadiotis G., 2015, *J. Geophys. Res. Space Phys.*, 120, 1607–1619
- Livadiotis G., McComas D., 2004, *J. Plasma Physics*, 80, 341
- Livadiotis G., McComas D. J., 2013, *Space Sci. Rev.*, 175, 183
- Livadiotis G., Desai M. I., Wilson L. B. I., 2018, *ApJ*, 853, 142
- Ma C., Summers D., 1998, *Geophys. Res. Lett.*, 25, 4099
- Mace R. L., Hellberg M. N., Treumann R. A., 1998, *J. Plasma Phys.*, 59, 393
- Maksimovic M., Pierrard V., Riley P., 1997, *Geophys. Res. Lett.*, 24, 1151
- Maksimovic M., et al., 2005, *Journal of Geophysical Research (Space Physics)*, 110, A09104
- Marsden R. G., Smith E. J., 2003, *News from the Sun's Poles* Courtesy of Ulysses
- Nauenberg M., 2003, *Phys. Rev. E*, 67, 036114
- Nauenberg M., 2004, *Phys. Rev. E*, 69, 038102
- Olbert S., 1968, in Carovillano R. D. L., McClay J. F., eds, *Astrophysics and Space Science Library Vol. 10, Physics of the Magnetosphere*. p. 641, [doi:10.1007/978-94-010-3467-8\\_23](https://doi.org/10.1007/978-94-010-3467-8_23)
- Paschmann G., Fazakerley A. N., Schwartz S. J., 1998, *ISSI Scientific Reports Series*, 1, 125
- Pierrard V., Lazar M., 2010, *Sol. Phys.*, 267, 153
- Pierrard V., Lazar M., Poedts S., Štverák Š., Maksimovic M., Trávníček P. M., 2016, *Sol. Phys.*, 291, 2165
- Scherer K., Fichtner H., Lazar M., 2017a, *EPL (Europhysics Letters)*, 120, 50002
- Scherer K., Fichtner H., Lazar M., 2017b, *EPL (Europhysics Letters)*, 120, 50002
- Scherer K., Lazar M., Husidic E., Fichtner H., 2019a, *ApJ*, 880, 118
- Scherer K., Fichtner H., Fahr H. J., Lazar M., 2019b, *ApJ*, 881, 93
- Schwabl F., 2013, *Statistical Mechanics*. Springer Science & Business Media
- Treumann R., Baumjohann W., 2014, *Frontiers in Physics*, 2, 49
- Treumann R. A., Jaroschek C. H., 2008, *Phys. Rev. Lett.*, 100, 155005
- Treumann R. A., Jaroschek C. H., Scholer M., 2004, *Physics of Plasmas*, 11, 1317
- Tsallis C., 1988, *J. Stat. Phys.*, 52, 479
- Tsallis C., 2004, *Phys. Rev. E*, 69, 038101
- Vasyliunas V. M., 1968, in Carovillano R. D. L., McClay J. F., eds, *Astrophysics and Space Science Library Vol. 10, Physics of the Magnetosphere*. p. 622, [doi:10.1007/978-94-010-3467-8\\_22](https://doi.org/10.1007/978-94-010-3467-8_22)
- Vasyliunas V. M., Siscoe G. L., 1976, *J. Geophys. Res.*, 81, 1247
- Webb S., Litvinenk V. N. o., Wang G., 2012, *Phys. Rev. STAB*, 15, 080701
- Yoon P. H., 2012, in Leubner M. P., Vörös Z., eds, *Multi-scale Dynamical Processes in Space and Astrophysical Plasmas*. Springer Berlin Heidelberg, Berlin, Heidelberg, pp 91–96
- Yoon P. H., 2014, *Journal of Geophysical Research (Space Physics)*, 119, 7074
- Yoon P. H., Seough J., Salem C. S., Klein K. G., 2019, *Phys. Rev. Lett.*, 123, 145101
- Zank G. P., Heerikhuisen J., Pogorelov N. V., Burrows R., McComas D., 2010, *ApJ*, 708, 1092
- de Avillez M. A., Gervasio J. A., Breitschwerdt D., 2018, *Astron. Astrophys.*, 616, A58
- Štverák Š., Trávníček P., Maksimovic M., Marsch E., Fazakerley A. N., Scime E. E., 2008, *Journal of Geophysical Research (Space Physics)*, 113, A03103

## APPENDIX A: SOME USEFUL PROPERTIES OF THE KUMMER- $U$ OR TRICOMI FUNCTION

### A1 Useful properties

The  $n$ th derivative with respect to  $x$  of  $U(a, b, x)$  is (Abramowitz & Stegun 1972, Eq. (13.4.22))

$$\frac{d^n}{d\xi^n} U(a, b, \eta\xi) = (-\eta)^n \frac{\Gamma(a+n)}{\Gamma(a)} U(a+n, b+n, \eta\xi), \quad (\text{A1})$$

and thus for the even moments we find for the derivative with respect to  $\xi$  (from Eq. (13))

$$\begin{aligned} U\left(\frac{3}{2}, \frac{5}{2} - \zeta, \eta\xi\right) \tilde{M}_{2n} &= \eta^n U\left(\frac{3}{2} + n, \frac{5}{2} + n - \zeta, \eta\xi\right) \\ &= (-1)^n \frac{\Gamma(\frac{3}{2})}{\Gamma(\frac{3}{2} + n)} \frac{d^n}{d\xi^n} U\left(\frac{3}{2}, \frac{5}{2} - \zeta, \eta\xi\right) \\ &= (-1)^n \frac{\sqrt{\pi}}{2\Gamma(\frac{3}{2} + n)} \frac{d^n}{d\xi^n} U\left(\frac{3}{2}, \frac{5}{2} - \zeta, \eta\xi\right), \quad (\text{A2}) \end{aligned}$$

and for the even moments

$$U\left(\frac{3}{2}, \frac{5}{2} - \zeta, \eta\xi\right) \tilde{M}_{2n+1} = \eta^{\frac{1}{2}+n} U(2+n, 3+n - \zeta, \eta\xi)$$

$$\begin{aligned}
 &= (-1)^n \eta^{\frac{1}{2}} \frac{\Gamma(2)}{\Gamma(2+n)} \frac{d^n}{d\xi^n} U(2, 3 - \zeta, \eta \xi) \\
 &= (-1)^n \eta^{\frac{1}{2}} \frac{1}{\Gamma(2+n)} \frac{d^n}{d\xi^n} U(2, 3 - \zeta, \eta \xi). \quad (\text{A3})
 \end{aligned}$$

Especially for the pressure we find:

$$\tilde{M}_2 = -\frac{2}{3} \frac{d}{d\xi} \ln \left[ U \left( \frac{3}{2}, \frac{5}{2} - \zeta, \eta \xi \right) \right]. \quad (\text{A4})$$

To evaluate Eq. (16) we go to the integral representation of the Kummer- $U$  or Tricomi function, see [Abramowitz & Stegun \(1972\)](#) Eq. (13.2.5):

$$\begin{aligned}
 \Gamma \left( \frac{n+3}{2} \right) U \left( \frac{n+3}{2}, \frac{n+5}{2}, 1 \right) &= \int_0^\infty e^{-t} t^{\frac{3+n}{2}-1} (1+t)^{\frac{5+n}{2}-\frac{3+n}{2}-1} dt \\
 &= \int_0^\infty e^{-t} t^{\frac{3+n}{2}-1} dt = \Gamma \left( \frac{n+3}{2} \right) \quad (\text{A5})
 \end{aligned}$$

and thus  $U \left( \frac{n+3}{2}, \frac{n+5}{2}, 1 \right) = 1$ .

## A2 Limits

The limits for low values of the third argument in the Kummer- $U$  function, can be found in [Abramowitz & Stegun \(1972, Eq.s \(13.5.10\) to \(13.5.12\)\)](#). In Table A1 the limits are more involved when we use  $\eta = \eta(\kappa)$  and  $\zeta = \zeta(\kappa)$  and want to study the case when  $\kappa \rightarrow 0$ . The recipes have to be checked individually.

Thus, for the limits when  $\xi \rightarrow 0$  we can combine case 1 and case 3 to:

$$U \left( \frac{3+n}{2}, \frac{5+n}{2} - \zeta, 0 \right) = \frac{\Gamma(\zeta - \frac{3+n}{2})}{\Gamma(\zeta)} \quad \text{if } \zeta > \frac{3+n}{2}, \quad (\text{A6})$$

and for the moments  $\tilde{M}^n$  we find:

$$\begin{aligned}
 \lim_{\xi \rightarrow 0} \eta^{\frac{n}{2}} \frac{U \left( \frac{n+3}{2}, \frac{n+5}{2} - \zeta, \xi \eta \right)}{U \left( \frac{3}{2}, \frac{5}{2} - \zeta, \xi \eta \right)} \\
 = \eta^{\frac{n}{2}} \frac{\Gamma(\zeta - \frac{3+n}{2})}{\Gamma(\zeta - \frac{3}{2})} \quad \text{if } \zeta > \frac{3+n}{2}. \quad (\text{A7})
 \end{aligned}$$

For the recipes  $(\kappa, \kappa+1, \xi = \text{const.})$  we have to use case 5 for the normalization, case 6 for the most probable speed and case 7 for the pressure:

$$\begin{aligned}
 \lim_{\kappa \rightarrow 0} \tilde{u}_p &= \lim_{\kappa \rightarrow 0} \sqrt{\kappa} {}^{[1]} \mathcal{U}^{[0]}(\kappa, \kappa+1, \xi) \\
 &= \lim_{\kappa \rightarrow 0} \sqrt{\kappa} \frac{\frac{1}{\kappa \xi} + \ln(\kappa \xi)}{\frac{\Gamma(\frac{1}{2}-\kappa)}{\Gamma(\frac{3}{2})(\kappa \xi)^{\frac{1}{2}-\kappa}} + \frac{\Gamma(-\frac{1}{2}+\kappa)}{\Gamma(\kappa+1)}} = \frac{1}{2\sqrt{\xi}} \quad (\text{A8})
 \end{aligned}$$

$$\begin{aligned}
 \lim_{\kappa \rightarrow 0} \tilde{P} &= \lim_{\kappa \rightarrow 0} \kappa {}^{[2]} \mathcal{U}^{[0]}(\kappa, \kappa+1, \xi) \\
 &= \lim_{\kappa \rightarrow 0} \kappa \frac{\frac{1}{2}-\kappa-(\kappa+1)\xi \kappa \Gamma(\frac{1}{2}-\kappa)}{\frac{\Gamma(\frac{5}{2})(\kappa \xi)^{\frac{1}{2}-\kappa}}{\Gamma(\frac{3}{2})(\kappa \xi)^{\frac{1}{2}-\kappa}} + \frac{\Gamma(-\frac{1}{2}+\kappa)}{\Gamma(\kappa+1)}} = \frac{1}{3\xi}, \quad (\text{A9})
 \end{aligned}$$

while for the recipes  $(\kappa - \frac{3}{2}, \kappa+1, \xi = \text{const.})$  we have to

choose case 2 for the normalization and cases 3 and 4 for the most probable speed and pressure, when  $\kappa \rightarrow \frac{3}{2}$ .

$$\begin{aligned}
 \lim_{\kappa \rightarrow \frac{3}{2}} \tilde{u}_p &= \lim_{\kappa \rightarrow \frac{3}{2}} \sqrt{\kappa - \frac{1}{2}} {}^{[1]} \mathcal{U}^{[0]}(\kappa - \frac{3}{2}, \kappa, \xi) \\
 &= \lim_{\kappa \rightarrow \frac{3}{2}} \sqrt{\kappa - \frac{3}{2}} \frac{\frac{\Gamma(\kappa)\Gamma(\kappa+1)}{\Gamma(3)} \frac{\Gamma(-\kappa)}{\Gamma(3)} ([\kappa - \frac{3}{2}] \xi)^{-\kappa}}{1 + \frac{\frac{3}{2}(\kappa - \frac{3}{2}) \xi \log([\kappa - \frac{3}{2}] \xi)}{\Gamma(3)}} = 0 \\
 \lim_{\kappa \rightarrow \frac{3}{2}} \tilde{P} &= \lim_{\kappa \rightarrow \frac{3}{2}} \kappa {}^{[2]} \mathcal{U}^{[0]}(\kappa - \frac{3}{2}, \kappa+1, \xi) \quad (\text{A10})
 \end{aligned}$$

$$= \lim_{\kappa \rightarrow \frac{3}{2}} (\kappa - \frac{3}{2}) \frac{\frac{2\gamma + \psi(\frac{5}{2}) + \ln([\kappa - \frac{3}{2}] \xi)}{-\Gamma(\frac{5}{2})}}{1 + \frac{\frac{3}{2}(\kappa - \frac{3}{2}) \xi \log([\kappa - \frac{3}{2}] \xi)}{\Gamma(3)}} = 0. \quad (\text{A11})$$

It can easily be seen that for the recipe  $(\kappa - \frac{3}{2}, \kappa+1, \frac{\kappa \xi}{\kappa - \frac{3}{2}})$  the double fraction becomes constant when  $\kappa \rightarrow \frac{3}{2}$ , and the factor in front of it goes to zero (similar for higher-order moments or different recipes).

For the recipe  $\kappa - \frac{3}{2}, \kappa+1, 0$  we can combine some of the factors:

$$\begin{aligned}
 \lim_{\kappa \rightarrow \frac{3}{2}} f(\kappa - \frac{3}{2}, \kappa+1, 0) \\
 = \lim_{\kappa \rightarrow \frac{3}{2}} \frac{\kappa \Gamma(\kappa)}{\Gamma(\kappa - \frac{1}{2}) (\kappa - \frac{3}{2})^{\frac{3}{2}} \sqrt{\pi^3} \Theta^3} \left( 1 + \frac{v^2}{(\kappa - \frac{3}{2}) \Theta^2} \right)^{-\kappa-1} \\
 = \frac{3}{2} \frac{\Gamma(\frac{3}{2})}{\Gamma(1) \sqrt{\pi^3} \Theta^3} \lim_{\kappa \rightarrow \frac{3}{2}} \frac{(\kappa - \frac{3}{2})^{\kappa+1}}{(\kappa - \frac{3}{2})^{\frac{3}{2}}} \left( \kappa - \frac{3}{2} + \frac{v^2}{\Theta^2} \right)^{-\kappa-1} \\
 = \frac{3}{2} \frac{\Gamma(\frac{3}{2})}{\Gamma(1) \sqrt{\pi^3} \Theta^3} \left( \frac{v^2}{\Theta^2} \right)^{-\frac{5}{2}} \lim_{\kappa \rightarrow \frac{3}{2}} \left( \kappa - \frac{3}{2} \right) = 0
 \end{aligned}$$

with  $\lim_{\kappa \rightarrow 0} \kappa^\kappa = 1$ .

## A3 The limits $\kappa \rightarrow \infty$

These limits are more complicated and it is the best to calculate the limiting distribution function and from that the limiting moments.

To calculate the upper limits of the normalization factor for the recipe  $(\kappa, \kappa+1, \xi^2)$ , the RKD, we use the original integral:

$$\begin{aligned}
 \lim_{\kappa \rightarrow \infty} \kappa^{\frac{3}{2}} U \left( \frac{3}{2}, \frac{3}{2} - \kappa, \kappa \xi^2 \right) \\
 = \lim_{\kappa \rightarrow \infty} \frac{1}{2\Gamma(\frac{3}{2})} \int_0^\infty e^{-\frac{\xi^2 v^2}{\Theta^2}} \left( 1 + \frac{v^2}{\kappa \Theta^2} \right)^{-\kappa-1} v^2 dv \\
 = \frac{1}{2\Gamma(\frac{3}{2})} \int_0^\infty e^{-\frac{1+\xi^2 v^2}{\Theta^2}} v^2 dv = \frac{\sqrt{\pi} \Theta^3}{4(1+\xi^2)^{\frac{3}{2}}},
 \end{aligned}$$

which has to be multiplied by  $4\pi$  because of the spherical volume element. In an analogous way one gets the upper limits of the other distribution functions.

Case 1:	$b < 0$	$\frac{(b+a\eta\xi)\Gamma(-b)}{-\Gamma(\zeta)}$
Case 2:	$b = 0$	$\frac{1+a\eta\xi\ln(\eta\xi)}{\Gamma(a+1)}$
Case 3:	$0 < b < 1$	$\frac{\Gamma(1-b)}{\Gamma(\zeta)} + \frac{\Gamma(b-1)(\eta\xi)^{1-b}}{\Gamma(a)}$
Case 4:	$b = 1$	$\frac{2\gamma+\psi(a)+\ln\eta\xi}{-\Gamma(a)}$
Case 5:	$1 < b < 2$	$\frac{\Gamma(b-1)}{\Gamma(a)(\eta\xi)^{b-1}} + \frac{\Gamma(1-b)}{\Gamma(\zeta)}$
Case 6:	$b = 2$	$\frac{1}{\Gamma(a)\eta\xi} + \frac{\ln\eta\xi}{\Gamma(a-1)}$
Case 7:	$b > 2$	$\frac{(b-2-\zeta\eta\xi)\Gamma(b-2)}{\Gamma(a)(\eta\xi)^{b-1}}$

**Table A1.** For  $U(a, b, x)$  with  $a = \frac{3+n}{2}$  and  $b = \frac{5+n}{2} - \zeta$ , where  $\gamma \approx 0.5772$  is the Euler constant, and  $\psi$  is the digamma function.

#### A4 The case $\eta \rightarrow 0$

From the above we find

$$\begin{aligned}
\lim_{\eta \rightarrow 0} \tilde{f} &= e^{-\xi(\kappa)\frac{v^2}{\Theta^2}} \lim_{\eta \rightarrow 0} \frac{1}{\eta^{\frac{3}{2}} U\left(\frac{3}{2}, \frac{5}{2} - \zeta, \eta\xi\right)} \left(1 + \frac{v^2}{\eta\Theta^2}\right)^{-\zeta} \\
&= e^{-\xi(\kappa)\frac{v^2}{\Theta^2}} \lim_{\eta \rightarrow 0} \frac{\eta^{\zeta - \frac{3}{2}}}{U\left(\frac{3}{2}, \frac{5}{2} - \zeta, \eta\xi\right)} \left(\eta + \frac{v^2}{\Theta^2}\right)^{-\zeta} \\
&= e^{-\xi(\kappa)\frac{v^2}{\Theta^2}} \lim_{\eta \rightarrow 0} \eta^{\zeta - \frac{3}{2}} \left(\eta + \frac{v^2}{\Theta^2}\right)^{-\zeta} \\
&\cdot \begin{cases} \frac{\sqrt{\pi}\eta^{\frac{3}{2}}\xi^{\frac{3}{2}}\Gamma(\zeta)}{2\eta^{\zeta}\Gamma(\frac{3}{2}-\zeta)\Gamma(\zeta)+\sqrt{\pi}\eta^{\frac{3}{2}}\xi^{\frac{3}{2}}\Gamma(\zeta-\frac{3}{2})} & \zeta > \frac{3}{2} \\ \frac{3\sqrt{\pi}}{4[1+\eta\xi*\ln(\eta\xi)]} & \zeta = \frac{5}{2} \\ \frac{2\Gamma(\zeta)}{(2\zeta-3\eta\xi-5)\Gamma(\zeta-\frac{5}{2})} & \zeta > \frac{5}{2} \end{cases} \\
&= 0. \tag{A12}
\end{aligned}$$

The first line goes to zero, because the denominator stays finite, while the numerator goes to zero. The same holds true for the second line ( $\lim_{x \rightarrow 0} x \ln(x) = 0$ ). The third row goes to zero because  $\zeta > 5$  and the denominator is positive. For  $\zeta \leq \frac{3}{2}$  the distribution function goes to infinity.

The moments are all proportional to  $\eta$  and go in general to zero, with the exceptional case discussed in subsection 4.2, where one moment can be chosen to be finite:

$$\begin{aligned}
\lim_{\eta \rightarrow 0} \tilde{M}_n &= \lim_{\eta \rightarrow 0} \eta^{\frac{n}{2}} \frac{U\left(\frac{n+3}{2}, \frac{n+5}{2} - \zeta, \eta\xi\right)}{U\left(\frac{3}{2}, \frac{5}{2} - \zeta, \eta\xi\right)} = \lim_{\eta \rightarrow 0} \eta^{\frac{n}{2}} \\
&\cdot \begin{cases} \frac{\sqrt{\pi}}{\Gamma(\frac{n+3}{2})} \frac{\Gamma(\frac{3+n}{2}-\zeta)(\eta\xi)^{\zeta-\frac{3+n}{2}}\Gamma(\zeta)+\Gamma(\zeta-\frac{3+n}{2})\Gamma(\frac{n+3}{2})}{2\Gamma(\frac{3}{2}-\zeta)(\eta\xi)^{\zeta-\frac{3}{2}}\Gamma(\zeta)+\sqrt{\pi}\Gamma(\zeta-\frac{3}{2})} & \zeta > \frac{3}{2} \\ \frac{\sqrt{\pi}\Gamma(\zeta)}{2\Gamma(\frac{n+3}{2})} \frac{2+\eta\xi(n+3)\ln(\eta\xi)}{2\Gamma(\frac{3}{2}-\zeta)(\eta\xi)^{\zeta-\frac{3}{2}}\Gamma(\zeta)+\sqrt{\pi}\Gamma(\zeta-\frac{3}{2})} & \zeta = \frac{5}{2} \\ -\frac{\Gamma(\zeta-\frac{5+n}{2})}{\Gamma(\zeta)} \left(\frac{3+n}{2}\eta\xi + \frac{5+n}{2} - \zeta\right) & \zeta > \frac{5}{2} \end{cases} \\
&= 0.
\end{aligned}$$

The fractions in the first and second line become constant when  $\eta \rightarrow 0$ , because the numerator and denominator have both a term independent of  $\eta$ , and thus the limit goes to zero. The factor in the third line has no dependence in the denominator on  $\eta$ , and thus vanishes also.

## APPENDIX B: THE INTEGRALS

We calculate the moments  $M_n = N_G^{-1} M'_n$  of the GKD by:

$$\begin{aligned}
M'_n &= 4\pi \int_0^\infty \left(1 + \frac{v^2}{\eta(\kappa)\Theta^2}\right)^{-\zeta(\kappa)} e^{-\xi(\kappa)\frac{v^2}{\Theta^2}} v^{2+n} dv \\
&= 2\pi\eta^{\frac{3+n}{2}} \Theta^{3+n} \int_0^\infty (1+x)^{-\zeta} e^{-\xi\eta x} x^{\frac{1+n}{2}} dx \\
&= 2\pi\eta^{\frac{3+n}{2}} \Theta^{3+n} \Gamma\left(\frac{n+3}{2}\right) U\left(\frac{n+3}{2}, \frac{n+5}{2} - \zeta, \xi\eta\right) \tag{B1}
\end{aligned}$$

If  $\xi = 0$ ,  $\zeta = \kappa + 1$ ,  $\eta = \kappa$  we obtain the SKD, etc., where the limiting cases (see Appendix A2) have to be taken into account whenever the argument  $\xi\eta$  of the Kummer- $U$  function approaches zero.

The normalization of the GKD is given by (including the factor  $4\pi$  from the spherical volume element)

$$N_G^{-1} = \tilde{M}_0 = \eta^{\frac{3}{2}} \Theta^3 \sqrt{\pi^3} U\left(\frac{3}{2}, \frac{5}{2} - \zeta, \xi\eta\right). \tag{B2}$$

#### B1 The entropy for the GKD

The normalized entropy  $S = S'/k_B$  ( $k_B$  is the Boltzmann constant and  $S'$  the entropy) is given by Boltzmann's H-theorem by (with  $4\pi$  from the spherical volume element) and neglecting the Gibbs correction (and the “-1” part)

$$S = - \int \int f \ln f d^3v d^3x \tag{B3}$$

and from the above

$$\begin{aligned}
S &= - \frac{4\pi}{\eta^{\frac{3}{2}} \Theta^3 \sqrt{\pi^3} U\left(\frac{3}{2}, \frac{5}{2} - \zeta, \xi\eta\right)} \int n_0 \int_0^\infty \left(1 + \frac{v^2}{\eta(\kappa)\Theta^2}\right)^{-\zeta(\kappa)} \\
&\cdot e^{-\xi(\kappa)\frac{v^2}{\Theta^2}} \ln \left( \frac{n_0 \left(1 + \frac{v^2}{\eta(\kappa)\Theta^2}\right)^{-\zeta(\kappa)} e^{-\xi(\kappa)\frac{v^2}{\Theta^2}}}{\eta^{\frac{3}{2}} \Theta^3 \sqrt{\pi^3} U\left(\frac{3}{2}, \frac{5}{2} - \zeta, \xi\eta\right)} \right) v^2 dv d^3x \\
&= -4\pi \int \int f \ln \left( \frac{n_0 \left(1 + \frac{v^2}{\eta(\kappa)\Theta^2}\right)^{-\zeta(\kappa)} e^{-\xi(\kappa)\frac{v^2}{\Theta^2}}}{\eta^{\frac{3}{2}} \Theta^3 \sqrt{\pi^3} U\left(\frac{3}{2}, \frac{5}{2} - \zeta, \xi\eta\right)} \right) v^2 dv d^3x \\
&= -4\pi \int \int f \ln \left( \frac{n_0}{\eta^{\frac{3}{2}} \Theta^3 \sqrt{\pi^3} U\left(\frac{3}{2}, \frac{5}{2} - \zeta, \xi\eta\right)} \right) v^2 dv d^3x \\
&\quad - 4\pi \int \int f \ln \left( \left(1 + \frac{v^2}{\eta(\kappa)\Theta^2}\right)^{-\zeta(\kappa)} e^{-\xi(\kappa)\frac{v^2}{\Theta^2}} \right) v^2 dv d^3x. \tag{B4}
\end{aligned}$$

In the first integral above the factor inside the  $\ln$  is independent of  $v$ . We split the first integral further by evaluating the logarithm. Then one integral is

$$\int n_0 \ln n_0 d^3x = N \ln \frac{N}{V} + N \int \frac{d \ln n_0}{dx} d^3x \approx N \ln n_0 + \text{const.}, \tag{B5}$$

which gives approximately the total number of particles  $N$ .

All other integrals are of the type  $\int n_0 \int G(v) dv d^3x$ , which gives the total number of particles  $N$  when integrating over



the volume, and the remaining parts are integrals with respect to  $v$ . With  $\tilde{S} = S/N - \text{const.}$  and with  $\tilde{f} = f/n_0$  we find then:

$$\tilde{S} = -4\pi \left( \ln n_0 - 3 \ln \Theta - \ln \left[ \eta^{\frac{3}{2}} \sqrt{\pi^3} U \left( \frac{3}{2}, \frac{5}{2} - \zeta, \xi \eta \right) \right] \right) - 4\pi \left( \underbrace{-\zeta \int_0^\infty \tilde{f} \ln \left[ 1 + \frac{v^2}{\eta \Theta^2} \right] v^2 dv}_{\text{The log-term}} - \frac{\xi}{\Theta^2} \int_0^\infty \tilde{f} v^4 dv \right).$$

The last expression is the pressure divided by  $n_0$  and we insert Eq. (9) (without  $n_0$ ). To continue we replace in the log-term 1 by  $\varepsilon$ , differentiate with respect to  $\varepsilon$ , expand into a Taylor series around  $\varepsilon = 1$ , integrate, and set  $\varepsilon = 1$ :

$$\begin{aligned} & -\zeta \int_\varepsilon \frac{\partial}{\partial \varepsilon} \int_0^\infty \tilde{f} \ln \left[ \varepsilon + \frac{v^2}{\eta \Theta^2} \right] v^2 dv d\varepsilon \Bigg|_{\varepsilon=1} \\ &= -\zeta \int_\varepsilon \int_0^\infty \tilde{f} \frac{1}{\varepsilon + \frac{v^2}{\eta \Theta^2}} v^2 dv d\varepsilon \Bigg|_{\varepsilon=1} \\ &= -\zeta \int_\varepsilon \int_0^\infty \tilde{f} \sum_{l=0}^{\infty} (-1)^l \frac{(\varepsilon - 1)^l}{(1 + \frac{v^2}{\eta \Theta^2})^{l+1}} v^2 dv d\varepsilon \Bigg|_{\varepsilon=1} \\ &= -\zeta \int_0^\infty \tilde{f} \sum_{l=0}^{\infty} (-1)^l \frac{(\varepsilon - 1)^{l+1} + (-1)^l}{(l+1)(1 + \frac{v^2}{\eta \Theta^2})^{l+1}} v^2 dv \Bigg|_{\varepsilon=1} \\ &= -\zeta \int_0^\infty \tilde{f} \sum_{l=0}^{\infty} \frac{1}{(l+1)(1 + \frac{v^2}{\eta \Theta^2})^{l+1}} v^2 dv \\ &= -\frac{\zeta}{\sqrt{\pi^3} \eta^{\frac{3}{2}} \Theta^3 U \left( \frac{3}{2}, \frac{5}{2} - \zeta, \eta \xi \right)} \cdot \int_0^\infty \sum_{l=0}^{\infty} \frac{1}{l+1} \left( 1 + \frac{v^2}{\eta \Theta^2} \right)^{-\zeta-l-1} e^{-\xi \frac{v^2}{\Theta^2}} v^2 dv \\ &= -\frac{\zeta}{2\pi} \sum_{l=0}^{\infty} \frac{1}{l+1} \frac{U \left( \frac{3}{2}, \frac{1}{2} - \zeta - l, \eta \xi \right)}{U \left( \frac{3}{2}, \frac{5}{2} - \zeta, \eta \xi \right)}, \end{aligned} \quad (\text{B6})$$

from which follows

$$\begin{aligned} \tilde{S} &= -4\pi \left( \ln n_0 - 3 \ln \Theta - \ln \left[ \eta^{\frac{3}{2}} \sqrt{\pi^3} U \left( \frac{3}{2}, \frac{5}{2} - \zeta, \xi \eta \right) \right] \right) \\ &- 4\pi \left( -\frac{\zeta}{2\pi} \sum_{l=0}^{\infty} \frac{1}{l+1} \frac{U \left( \frac{3}{2}, \frac{1}{2} - \zeta - l, \eta \xi \right)}{U \left( \frac{3}{2}, \frac{5}{2} - \zeta, \eta \xi \right)} \right. \\ &\quad \left. - \frac{2\xi \eta}{3} \frac{U \left( \frac{5}{2}, \frac{7}{2} - \zeta, \xi \eta \right)}{U \left( \frac{3}{2}, \frac{5}{2} - \zeta, \xi \eta \right)} \right). \end{aligned} \quad (\text{B7})$$

For the Maxwellian  $\zeta = 0, \xi = \eta = 1$  we find from Eq. (B7) and the corresponding limits:

$$\tilde{S} = -4\pi \ln n_0 + 12\pi \ln \Theta + \frac{3}{2} \ln \pi + \frac{8\pi}{3} \quad (\text{B8})$$

or  $\frac{\tilde{S}}{4\pi} = 3 \ln \Theta - \ln n_0 + \text{const.}$

Replacing  $\Theta$  by the thermal speed we get the Maxwellian entropy (up to a constant).

Even if the Maxwellian part disappears ( $\xi = 0$ ), we get a solution because of ( $\zeta > \frac{3}{2}$ ), and thus the second moment (pressure) exists (last term of Eq. B7).

### APPENDIX C: THE INTEGRALS FOR THE DEBYE LENGTH

The Debye length is defined via the Poisson equation

$$\Delta \Phi = -\frac{1}{\varepsilon_0} \left( q_T \delta(r) + \sum_s q_s n_s(r) \right), \quad (\text{C1})$$

where  $\varepsilon_0$  is the vacuum permittivity,  $q_T$  the charge of a test particle,  $n_s$  the disturbed number density of particle species  $s$  (0th moment of the corresponding disturbed distribution function) and  $q_s$  their charge. Because of charge neutrality  $\sum_s q_s n_s = q_e n_{0,e} + q_i n_{0,i} = 0$  (we only discuss electrons and positively charged ions (protons), which is stated in the last step). We rearrange Eq. (C1) to

$$\Delta \Phi - \frac{1}{\varepsilon_0} \sum_s q_s n_s(r) = -\frac{q_T}{\varepsilon_0} \delta(r) \quad (\text{C2})$$

and find (for each species)

$$\Delta \Phi + \frac{1}{\varepsilon_0} \sum_s q_s n_s(r) \approx \Delta \Phi + \frac{1}{\varepsilon_0} \sum_s n'_s \frac{q_s^2 \Phi}{m_s \Theta_s^2} = -\frac{q_T}{\varepsilon_0} \delta(r), \quad (\text{C3})$$

where  $m_s$  and  $\Theta_s$  are the mass and thermal core speed for each species, respectively. The Debye length  $\Lambda$  is then defined as

$$\Lambda^{-2} = \Lambda_e^{-2} + \Lambda_i^{-2} = \frac{q_e^2 n'_e}{\varepsilon_0 m_e \Theta_e^2} + \frac{q_i^2 n'_i}{\varepsilon_0 m_i \Theta_i^2} \quad (\text{C4})$$

(for electrons and ions only). The 0th-order moment (number density) of the perturbed distribution functions is calculated in Appendix C. These perturbed number densities  $n_p$  are developed into a Taylor series up to the first order in  $\chi = \frac{q\Phi}{m\Theta^2}$  (neglecting the index  $s$ ) and yield, in general:

$$n_s = n_0 \left( 1 + \frac{q\Phi}{m\Theta^2} n'_s \right), \quad (\text{C5})$$

where  $n'_s$  is a factor different for each distribution function. By inserting Eq. (C5) in Eq. (C3) it becomes evident that the first part of Eq. (C5) cancels for ions and electrons species because of the charge neutrality.

To calculate the Debye length, we replace the velocity by the kinetic energy  $E_{kin}$  and add as a perturbation the potential energy  $V$  (or “chemical” potential as in Treumann et al. (2004) and Fahr & Heyl (2016)) of the test particle:

$$v^2 \rightarrow \frac{E_{kin}}{2m_s} \rightarrow \frac{E_{kin} + V}{2m_s}, \quad (\text{C6})$$

where  $V = q_s \Phi$  is the electric potential of a test charge, and  $\pm v_\Phi^2 = q_s \Phi / (2m_s)$  is the corresponding speed depending on the charge sign. We always assume that  $v_\Phi^2 / \Theta^2$  is small. In contrast to the previous attempts in literature, we replace the Maxwellian temperature by the the core speed  $\Theta$ . The integrals (zerth moments) corresponding to the perturbed distribution functions from Table 4 and their limits found in Table 5 are discussed in the Appendix C. In the Debye length the corresponding  $\kappa$ -pressure (or temperature) appears as a correction, except for the SKD and recipe ( $\kappa - \frac{3}{2}, \kappa + 1, 0$ ).

We do not follow the Debye-Hückel theory, because we want to include collisionless plasmas, thus we will use the approach by [Krall & Trivelpiece \(1973\)](#).

### C1 The Debye length after Krall & Trivelpiece

In [Krall & Trivelpiece \(1973\)](#), chapter 11.1 a shielding length is calculated on the basis of a Vlasov-plasma, but for arbitrary distributions (not too far away from equilibrium), splitting the distributions functions in

$$f_s = f_{0,s} + f_{1,s}, \quad (\text{C7})$$

where  $f_{0,s}$  is the unperturbed distribution and  $f_{1,s}$  the perturbation of the distribution function for species  $s$ . In the following we drop the index  $s$ .

Following ([Krall & Trivelpiece 1973](#)) we have in lowest order that a moving test charge follows a straight line

$$\vec{x}' = \vec{x}'_0 - \vec{v}'t, \quad (\text{C8})$$

where  $\vec{v}'$  is a uniform velocity and  $\vec{x}'_0$  is the location of the test charge at  $t = 0$ . Then the potential can be written as:

$$\nabla^2 \Phi = \frac{1}{\epsilon} q \delta(\vec{x} - \vec{x}'_0 - \vec{v}'t) + \frac{1}{\epsilon} n \quad (\text{C9})$$

with

$$n = \sum_s q_s \int f_s d^3v. \quad (\text{C10})$$

Note: In our notation the number density  $n_s$  is part of the distribution function  $f_s$ . The plasma distribution function  $f_s$  satisfies the Vlasov equation:

$$dt f_s + (\vec{v} \cdot \vec{\nabla}) f_s - \frac{q_s}{m_s} (\vec{\nabla} \Phi) \cdot \vec{\nabla}_v f_s = 0, \quad (\text{C11})$$

assuming that the plasma in absence of the test charge is field free and uniform. Furthermore, we assume that the perturbation is weak, and the distribution can be linearized:

$$f_s = f_{s,0}(\vec{v}) + f_{s,1}(\vec{x}, \vec{v}, t) \quad (\text{C12})$$

$$\frac{\partial f_{s,1}}{\partial t} + (\vec{v} \cdot \vec{\nabla}) f_{s,1} = \frac{q_s}{m_s} (\vec{\nabla} \Phi) \cdot \vec{\nabla}_v f_s$$

$$\sum_s n_{s,0} q_s \int f_{s,0} d^3v = 0.$$

The Fourier-Laplace-transform (and the back-transform) of the perturbed Vlasov equation Eq. (C12) are given by

$$(\text{C13})$$

$$\tilde{h}(\vec{k}, \vec{v}, \omega) = \int h(\vec{r}, \vec{v}, t) e^{-i(\omega t + \vec{k} \cdot \vec{r})} dt d^3r,$$

$$h(\vec{r}, \vec{v}, t) = \int \tilde{h}(\vec{k}, \vec{v}, \omega) e^{i(\omega t + \vec{k} \cdot \vec{r})} d\omega d^3k.$$

We further assume that the test particle is at rest at  $\vec{r} = \vec{0}$ , and find:

$$-i\vec{k} \cdot \vec{v} \tilde{f}_{s,1} = -i \frac{q_s \Phi}{m_s} (\vec{k} \cdot \vec{\nabla}_v \tilde{f}_{s,0}). \quad (\text{C14})$$

For isotropic distribution functions we can change to spherical coordinates, and assuming that the integral does not depend on  $d\varphi$  and  $d\vartheta$ , replacing  $\vec{k} \cdot \vec{v} = kv \cos \xi$ , the Fourier-transform then simplifies to:

$$-ikv \cos \xi \tilde{f}_{s,1} = -ik \cos \xi \frac{v q_s \Phi}{m_s} \frac{d}{dv} \tilde{f}_{s,0}, \quad (\text{C15})$$

where also the velocity dependence was changed to spherical coordinates. From the above equation we find, after the back-transformation:

$$f_{s,1} = \frac{q_s \Phi}{m_s} \frac{1}{v} \frac{d}{dv} f_{s,0}. \quad (\text{C16})$$

Inserting in Eq. (C9) and solving the equation we find

$$\nabla^2 \Phi - \left[ -\sum_s \frac{n_s q_s^2}{\epsilon m_s} \int \frac{1}{v} \frac{d}{dv} f_{s,0} d^3v \right] \Phi = \frac{1}{\epsilon} \delta(\vec{r}), \quad (\text{C17})$$

where the Debye length for collisionless distribution functions is

$$\frac{1}{\Lambda_D^2} = -\sum_s \frac{n_s q_s^2}{\epsilon m_s} \int \frac{1}{v} \frac{d}{dv} f_{s,0} d^3v = \sum_s \Lambda_{D,s}^{-2} \quad (\text{C18})$$

$$(\text{C19})$$

and finding that

$$\frac{1}{\Lambda_D^2} = -\sum_s \omega_{p,s}^2 \int \frac{1}{v} \frac{\partial f_{0s}}{\partial v} d^3v. \quad (\text{C20})$$

We stay here with the name Debye length rather than using shielding length. We also point out that this Debye length is only valid for test charges at rest. For moving test charges the shielding is also discussed by ([Krall & Trivelpiece 1973](#), chapter 11.1). The term  $\omega_{p,s}^2 = \frac{4\pi n_s e^2}{m_s}$  is the plasma frequency of species  $s$ .

Inserting  $f_{0,s} = \tilde{f}$  and dropping the index  $s$  we have

$$\begin{aligned} \Lambda^{-2} &= \omega_p \frac{2\pi}{\sqrt{\pi^3} \eta^{\frac{3}{2}} \Theta^3 U \left( \frac{3}{2}, \frac{5}{2} - \zeta, \eta \xi \right)} \\ &\left( \frac{2\zeta}{\eta \Theta^2} \int_0^\infty \left[ \left( 1 + \frac{v^2}{\eta \Theta^2} \right)^{-\zeta-1} e^{-\xi \frac{v^2}{\Theta^2}} \right] v^2 dv \right. \\ &\left. + \frac{2\xi}{\Theta^2} \int_0^\infty \left[ \left( 1 + \frac{v^2}{\eta \Theta^2} \right)^{-\zeta} e^{-\xi \frac{v^2}{\Theta^2}} \right] v^2 dv \right) \\ &= 2\Lambda_M^{-2} \left( \frac{\zeta}{\eta} \frac{U \left( \frac{3}{2}, \frac{3}{2} - \zeta, \eta \xi \right)}{U \left( \frac{3}{2}, \frac{5}{2} - \zeta, \eta \xi \right)} + \xi \right). \end{aligned}$$

The additional factor comes from our definition of the Maxwellian.

This paper has been typeset from a  $\text{\TeX}/\text{\LaTeX}$  file prepared by the author.